

NEUTRONIC DESIGN AND OPTIMIZATION OF A POROUS-FUEL,
HIGH-TEMPERATURE, GAS-COOLED REACTOR FOR SPACE POWER AND
PROPULSION APPLICATIONS

By

EDDY PEREZ CARDENTY

A THESIS PRESENTED TO THE GRADUATE SCHOOL
OF THE UNIVERSITY OF FLORIDA IN PARTIAL FULFILLMENT
OF THE REQUIREMENTS FOR THE DEGREE OF
MASTER OF SCIENCE

UNIVERSITY OF FLORIDA

2005

Copyright 2005

by

Eddy Perez Cardentey

To my grandfather, Victor Cardentey Gonzalez, and the memory of my late grandmother,
Amparo Rodriguez Chavez.

ACKNOWLEDGMENTS

I would like to thank Dr. Samim Anghaie, Prof. James Tulenko, and Dr. Pasquale Sforza for serving on my supervisory committee. I express my sincere gratitude to Dr. Samim Anghaie, who provided excellent tutoring as my committee chair and showed constant patience and support. I acknowledge Reza Gouw for his invaluable cooperation in determining fuel isotopic composition and density. I thank my family for their love, support, and understanding; and my friends for always being here for me.

TABLE OF CONTENTS

	<u>page</u>
ACKNOWLEDGMENTS	iv
LIST OF TABLES	vii
LIST OF FIGURES	viii
ABSTRACT	x
CHAPTER	
1 INTRODUCTION	1
Nuclear Space Reactors	1
Foam Fuel Space Nuclear Reactor	3
Objectives	4
2 METHODOLOGY	5
Monte Carlo Method	5
Monte Carlo N-Particle Code	7
Monte Carlo Burnup and Oak Ridge Isotope Generation Codes	9
3 REACTOR OPTIMIZATION	10
Optimization of Physical Dimensions	10
Uranium Density Optimization and Reactor Temperature Defects	12
Optimum Reactor Solutions	17
Burnup Study	20
Control Drum Design and Rotation	24
Alternate Moderator Composition	28
4 REACTOR SAFETY AND SHIELDING	33
Infinite Reflector Study	34
Water Immersion Study	36
Operational Reactor Flux	40
Reactor Shielding	42
5 SUMMARY AND CONCLUSIONS	47

Summary of Results.....	47
Data Summary and Delivery as Maplets	48
Future Work.....	50

APPENDIX

A INPUT FILE FOR MCNP	51
B INTERPOLATING ALGORITHM IN MAPLE.....	54
LIST OF REFERENCES.....	55
BIOGRAPHICAL SKETCH	56

LIST OF TABLES

<u>Table</u>	<u>page</u>
3-1 Multiplication factor and temperature defects for the fuel, moderator and reflector for reactor with 0.35 gU/cc density.	14
3-2 Re-optimized core multiplication factor and temperature defects for the fuel, moderator and reflector for reactor with 0.35 gU/cc.....	16
4-1 Elemental composition of water-fuel mixture.....	36
4-2 Multiplication factor for the system surrounded by varying thicknesses of boron carbide foil, with a boron carbide plug in the central fuel element and in all fuel elements.....	37

LIST OF FIGURES

<u>Figure</u>	<u>page</u>
1-1 Foam fuel space reactor.....	3
2-1 Absorption and scattering cross sections for yttrium hydride from ENDF-60 and ENDL-92 cross-section libraries.....	8
3-1 Reactor optimization by varying the center-to-flat distance in the fuel lattice.	11
3-2 Multiplication factor versus lattice radius for the 1.5 g/cc U density reactor.	12
3-3 Multiplication factor versus Uranium density.....	13
3-4 Multiplication factor versus lattice radius for the 0.35 gU/cc reactor.....	15
3-5 Reactivity worth of the reactor at operating temperature.....	17
3-6 Multiplication factor versus Uranium density and lattice radius.	18
3-7 Optimized lattice radius for uranium densities between 0.1 gU/cm ³ and 1.5 gU/cm ³	18
3-8 Optimized k-effective as a function of uranium density.	19
3-9 Multiplication factor vs. burnup for 8-hr burn at 500 kW thermal power.	21
3-10 Core isotopic inventory for approach burn.	21
3-13 Control drums with variable boron carbide thickness.....	24
3-14 Multiplication factor versus B ₄ C sliver thickness.	25
3-15 Multiplication factor versus control drum rotation.	26
3-16 Reactivity worth for control drum rotation.	27
3-17 Control drum rotation as a function of full power days.	27
3-18 Critical k-effective for a 140-day burn.....	28
3-19 Absorption and scattering cross sections for YH ₂ and ZrH ₂	29

3-20	Multiplication factor vs. lattice radius for various uranium densities.....	30
3-21	Multiplication factor versus lattice radius and uranium density..	30
3-22	Optimized k-effective vs. uranium density for both moderator types.....	31
4-1	Convergence on k-effective for shutdown optimized system in an infinite reflector.	34
4-2	Neutron flux in the reactor with inner control plugs in all fuel elements, normalized to particle histories.	38
4-3	Neutron flux in the reactor with inner control plugs and shells in all fuel elements, normalized to particle histories.	39
4-4	Thermal neutron flux in the reactor core from 0 to 0.625 eV	41
4-5	Power peaking factors in the fuel.....	42
4-6	Normalized neutron flux in axial BeO reflector.....	43
4-7	Attenuation percent across the LiBH ₄ shield, ± standard error corresponding to one standard deviation.....	44
5-1	Data delivery maplet for the YH ₂ moderated reactor.	49

Abstract of Thesis Presented to the Graduate School
of the University of Florida in Partial Fulfillment of the
Requirements for the Degree of Master of Science

NEUTRONIC DESIGN AND OPTIMIZATION OF A POROUS-FUEL,
HIGH-TEMPERATURE, GAS-COOLED REACTOR FOR SPACE POWER AND
PROPULSION APPLICATIONS

By

Eddy Perez Cardentey

August 2005

Chair: Samim Anghaie

Major Department: Nuclear and Radiological Engineering

Nuclear reactors are currently being considered for space power and propulsion applications. The system we examined uses a porous fuel matrix as the thermal interchange medium. Its intended use is in thermal propulsion systems, but it can also be applied to electric propulsion systems, and as a source of auxiliary power. The reactor would be used as a power source for interplanetary robotic or manned missions.

Our goal was to develop an optimized relation between fuel density and reactor dimensions. We used the Monte Carlo N-Particle code version 5 (MCNP5) to analyze the system at various points. We used a Maple algorithm to interpolate the data and mathematically maximize it. We used the Monte Carlo Burnup code (MONTEBURNS) to calculate burnup.

Results showed that the optimized system can easily be made critical. Extended burns are possible by adding excess reactivity by increasing the uranium density in the fuel matrix. However, the moderator shows a positive reactivity coefficient, causing the

hot core to have a higher k-effective than the cold core. Nonetheless, control drums were engineered to shut down the reactor even in a hot core.

Safety and shielding were evaluated. We determined that a water-immersion scenario would significantly increase reactivity, making the system supercritical. This situation was mitigated by using of safety plugs and shells in all fuel elements during launch. We used LiBH_4 as a shielding material, and it was very effective for this purpose. Additional attenuation was also observed in the BeO reflector surrounding the reactor.

Overall, the studied design shows that a critical system can be assembled. Safety and control were addressed and the system was shown to remain critical during operation and subcritical in accident scenarios. The positive reactivity coefficient raises some concern, however, warranting further study in this area.

CHAPTER 1 INTRODUCTION

Space propulsion requirements for manned interplanetary missions in the near future cannot be met with conventional methods. Chemical rockets have limited thrust and maneuverability, and because of the limited energy stored in chemical bonds, most of the mass in these systems is occupied by fuel. After using most of the fuel to escape earth orbit, little is left to generate sufficient acceleration to reach other planets in a reasonable amount of time to undergo a manned mission. Nuclear reactors are the only power source capable of delivering the thrust and onboard power required for such missions in a small, lightweight, affordable package.

One such reactor concept is under development in a partnership among Ultramet, Sandia National Labs, and the University of Florida. A team of researchers from these institutions are working under a joint National Aeronautics Space Administration (NASA) Small Business Technology Transfer (STTR) project, funded through Marshall Space Flight Center, to develop a new high-temperature tricarbide fuel matrix.

Nuclear Space Reactors

Nuclear reactors, such as those used for nuclear thermal propulsion, are quite different from previous chemical propulsion methods. In a chemical rocket, fuel and oxidizer are mixed in a combustion chamber, and expelled out from a nozzle; thus the fuel and propellant are the same. Once the propellant is exhausted, the main power source also vanishes. In addition, the very large quantities of propellant needed simply to leave earth orbit add tremendous size and weight to the vehicle. In the case of a

nuclear-powered ship, the fuel stays in the reactor while the propellant passes through it, picks up energy, and exits through the nozzle. A nuclear reactor can achieve much higher temperatures than combustion chambers in conventional rockets. Combined with the use of low-atomic-weight propellants (such as hydrogen), this results in more than twice the specific impulse than that obtained through chemical means. As a result, a trip to mars that would take 600 days with conventional rockets can be cut down to 200 days [1]. In addition to being a more efficient way to generate thrust, when the propellant is exhausted, the nuclear reactor can be used to generate electrical power for onboard components.

Space nuclear power first came under study in the 1960s under President John F. Kennedy. The cold war was raging and the race to the moon was well underway. A variety of projects (such as the NRX and project Rover), were aimed at using nuclear thermal propulsion to power a rocket through space. Other projects, such as the SNAP series, were aimed at developing nuclear reactors to provide auxiliary power. The program was such a success that a reactor was built and put in orbit (the SNAP-10A). Although a fault in the electrical system caused it to shut down soon into the mission, its twin system continued to operate on earth for a year, demonstrating the technical capabilities of the system.

Project Rover and most of the space nuclear program were terminated in 1973, after the moon landings left the space program with no immediate mission. More than 30 years elapsed before interest in interplanetary travel prompted new designs and developments.

Foam Fuel Space Nuclear Reactor

The team from the University of Florida, Sandia, and Ultramet is developing a new type of fuel for space propulsion applications. The fuel in this case is a high-temperature tricarbide matrix composed of ZrC, NbC, and UC in an open-cell reticulated foam element [2]. Unlike past designs, the coolant passes through the fuel in this case, rather than around it. This makes a much larger surface area available for heat transfer [3]. Thus, the coolant can be brought to a higher temperature while minimizing the fuel centerline temperature.

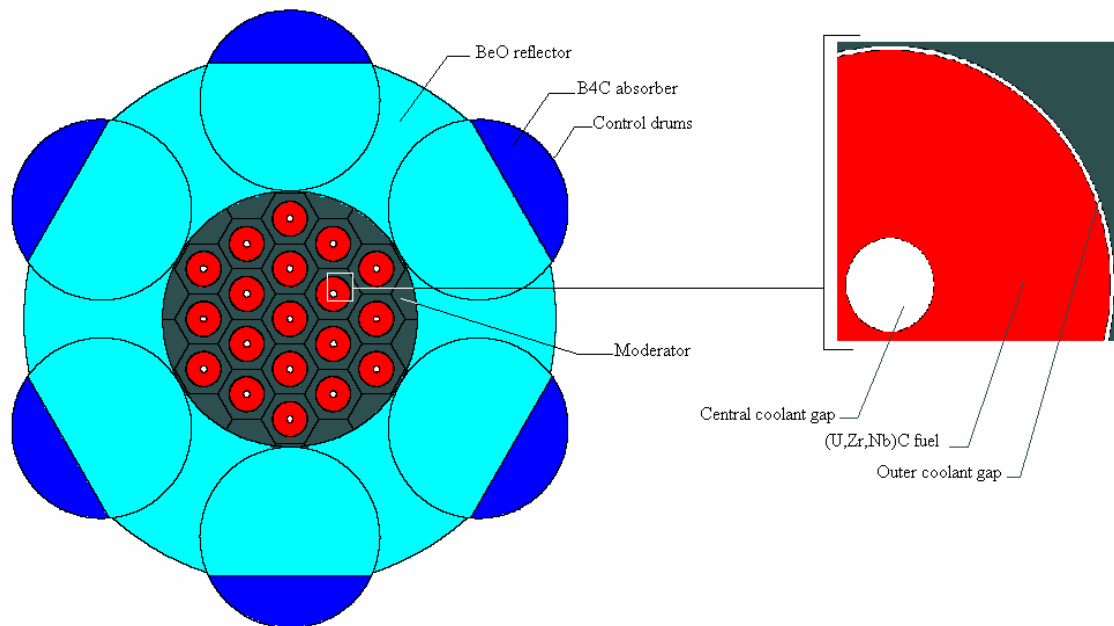


Figure 1-1. Foam fuel space reactor.

Figure 1-1 shows the overall layout of the reactor. The reactor is surrounded by 20 cm of BeO reflector radially and axially. The fuel has an inner radius of 0.5 cm, and an outer radius of 2.5 cm; and the thickness of the axial coolant gap is 0.049 cm. None of the other physical parameters are set, since they are the focus of the optimization procedure.

In this concept, the coolant flows radially inward through the fuel, toward the central coolant gap. Once there, it flows out of the reactor. Criticality is controlled by rotating the control drums. The moderator material is ZrH_2 . We also explored YH_2 as an alternate moderator.

Objectives

Our goal was to simulate the behavior of multiple variations of the system shown in Figure 1-1, and determine the optimum design parameters. The systems were modeled on MCNP5. We used MONTEBURNS to calculate burnup. Our study focused mainly on the following objectives.

- **Optimized reactor dimensions:** We determined the optimum dimensions for attaining maximum k-effective for varying uranium densities in the fuel, by mathematically maximizing functions obtained through interpolation algorithms derived from the data.
- **Reactor burnup:** We analyzed the system using MONTEBURNS to determine isotopic composition through the burn, and to determine length of time at which the system could be run.
- **Reactor safety:** Various scenarios were explored, arising from an unsuccessful launch. These scenarios made the system supercritical, and solutions were found to prevent catastrophe.

CHAPTER 2 METHODOLOGY

Our study focused on the neutronic evaluation of several variants of a critical system. As such it made heavy use of deterministic and probabilistic neutron transport methods. For this purpose, we decided to use existing codes that were proven to be robust and reliable. The main code implemented was Monte Carlo N-Particle code version 5 (MCNP5), developed by Los Alamos National Lab. It is a probabilistic neutron transport code used to trace particle interactions. We used MCNP5 to obtain criticality, as well as in conjunction with MONTEBURNS to model burnup. The latter is actually a linker between MCNP5 and ORIGEN2, rather than an actual code, while MCNP5 is the de facto Monte Carlo method code.

Monte Carlo Method

The Monte Carlo method is used to duplicate a statistical process in a theoretical manner. It uses a random sampling technique to model a random process that has a predefined probability distribution, such as the fission process, neutron scattering, and absorption. This is achieved through the Fundamental Formulation of Monte Carlo, whereby the probability density function is integrated as $\int_a^b \text{pdf}(x) \beta dx = 1$.

After integration, the resulting function is algebraically manipulated by inverting it so the normalization constant, $\beta = 1 / \int_a^b \text{pdf}(x) dx$ is solved for. The function is then expressed in a form such that the dependent variable is sampled as a function of a random number by first taking the indefinite integral $\int_a^{x_0} \text{pdf}(x) \beta dx = \eta$. The resulting

equation is then solved for x_0 as a function of the random number eta. This can be shown with the process of randomly sampling the distance traveled before interaction by a particle from the attenuation coefficient. In this case, the pdf is defined as $p(r) = \Sigma e^{(-\Sigma r)}$ where Sigma is the attenuation coefficient. The function can then be normalized by taking the integral $\int_0^{\infty} \Sigma e^{(-\Sigma r)} dr = 1$ and obtaining $\beta = -\Sigma / \left(\left(\lim_{r \rightarrow \infty} \frac{1}{e^{(\Sigma r)}} \right) - 1 \right)$. Knowing that the limit in the denominator approaches zero, we know that $\beta = \Sigma$. Thus, $\int_0^x \Sigma e^{(-\Sigma r)} dr = \eta$, $1 - e^{(-\Sigma x)} = \eta$, and $x = -\frac{\ln(1 - \eta)}{\Sigma}$ where eta is a random number between zero and one and x is the sampled flight distance. Since eta is a random number, the sampled distance can be rewritten as $x = -\ln(\eta) / \Sigma$.

This method can be used to simulate the interactions of particles with materials, making it particularly useful to simulate problems too complex to be solved with deterministic methods. To achieve this, the individual probabilistic events that make up a process are simulated sequentially. Each event's respective probability distribution is used to randomly sample the outcome of events along the way. Particle histories are created by following events particles undergo. By simulating a very large number of histories, the statistical behavior of the system as a whole emerges. The uncertainty is the decreased by increasing the number of histories.

The Monte Carlo method is used in nuclear engineering to obtain system parameters such as multiplication factor, spatial flux and neutron lifetimes, but it is also used in a variety of other fields. Nuclear medicine uses it to simulate radiation transport in the human body, for imaging and therapy applications. Electrical engineers make wide use of the Monte Carlo method for circuit analysis and semiconductor charge carrier transport. In addition, civil, industrial and a variety of other engineering disciplines use it

to simulate problems in their respective fields. Monte Carlo has even been used by economists to study and predict trends in the financial market. In fact, any problem that can be described as an aggregate of probabilities from individual events can be simulated through the use of the Monte Carlo method.

This work made use of the Nuclear Engineering application of the Monte Carlo method. Namely, we used it to obtain the behavior of neutron flux and multiplication factors and their variation as a function of variations in the material and geometric properties of the system. We used MCNP5 for this purpose, since it is a very robust and versatile implementation of the Monte Carlo method.

Monte Carlo N-Particle Code

The Monte Carlo N-Particle code (MCNP) was first released in 1977, emerging from Monte Carlo method developments undertaken at Los Alamos National Laboratory (LANL) during World War II. It has been under continuous development since then. The latest releases are MCNP5, developed by the Diagnostics Applications group, and MCNPX, developed by the Applied Physics Division [4]. All development work has been done at LANL. While both codes can be used for any nuclear or radiological application, MCNPX is geared towards high energy physics, while MCNP5 is geared towards reactor analysis and health physics applications.

MCNP5 uses continuous-energy nuclear and atomic cross-section data libraries. The primary sources are LANL's Evaluated Nuclear Data File (ENDF), Lawrence Livermore National Laboratory's Evaluated Nuclear Data Library (ENDL), Advanced Computational Technology Initiative (ACTI) and Evaluated Photon Data Library (EPDL), among others. In addition, the user has the option to use his or her custom libraries and cross section data. Nuclides are oftentimes furnished with more than one

available data library, primarily because data has originated from different sources. In addition, some data is processed at different temperatures to provide proper Doppler broadening. Input is fed into MCNP via an input file. Appendix A shows one of such input files used in this study, illustrating the general structure of the input.

It is imperative to pay close attention to the accuracy of the data used in any study. Case in point; there is a significant difference in the absorption cross-section for yttrium between LANL's ENDL-60 and LLNL's ENDF-92 cross-section files. This was noticed when one case run with the yttrium library from Los Alamos resulted in a value for k -effective that was 12.3% higher than that obtained with the library from Lawrence Livermore. After plotting the data, (Figure 2-1), and further evaluation, a conclusion was made that Los Alamos's cross section file contained correct values for yttrium.

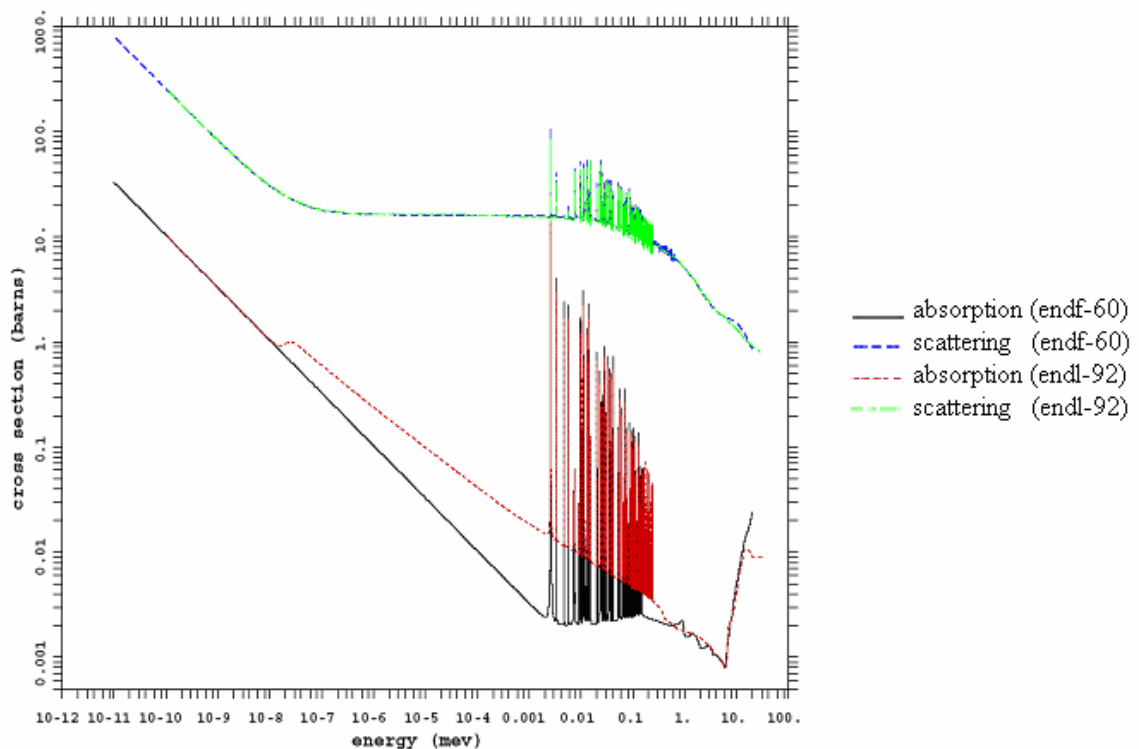


Figure 2-1. Absorption and scattering cross sections for yttrium hydride from ENDF-60 and ENDL-92 cross-section libraries.

Fortunately, this error was caught early in the research, but regrettably, a large amount of data originating from a series of rather lengthy batch runs was deemed invalid and had to be discarded. This extended the length of time work was conducted and postponed its termination. Had this research been part of time critical work for a mission, the delay would have certainly been most detrimental.

Monte Carlo Burnup and Oak Ridge Isotope Generation Codes

The Oak Ridge Isotope Generation code version 2 (ORIGEN2), developed by Oak Ridge National Laboratory (ORNL), is a widely used code to calculate the buildup, decay and processing of radioactive materials. ORIGEN2 is the successor to ORIGEN, and the newer code has updated reactor models cross-sections, fission product yields decay data, and the code itself.

The Los Alamos National Laboratory's Monte Carlo Burnup code (MONTEBURNS) is a link between MCNP and ORIGEN2. It is used to obtain isotopic compositions and criticality in a system as a function of time and burnup. This is achieved through the use of a Perl script that executes MCNP, ORIGEN2 and the fortran 77 code monteb.f. Monteb.f, or once compiled, monteb.exe, manipulates the output and input files between MCNP and ORIGEN2 and creates a fully automated burnup tool. MONTEBURNS uses MCNP primarily to obtain one-group cross sections and fluxes that are used by ORIGEN2 to perform burnup calculations [5]. Once completed, new isotopic compositions from ORIGEN2 are passed back into MCNP to obtain new fluxes and cross sections and initiate another burnup cycle.

CHAPTER 3 REACTOR OPTIMIZATION

The reactor optimization process was performed in the system moderated with Zirconium Hydride. A physical optimization was first performed so as to obtain the optimum parameters. Subsequently, the fuel composition was optimized so as to obtain a critical system with the minimum Uranium density. This is important because the tricarbide fuel matrix becomes more robust as the Uranium concentration decreases.

Optimization of Physical Dimensions

To find the optimum reactor dimensions, several models were created, by varying the flat-to-flat distance of the elements making up the fuel lattice. The reflector thickness was kept at a thickness of 20 cm at all times. It enveloped the right cylindrical reactor at all times. As the flat-to-flat distance was varied, the radius of the core changed, subsequently the axial dimension of the core expanded as well so as to keep it a right circular cylinder. The enveloping reflector dimensions changed as well as a function of the fuel lattice radius so as to maintain a constant 20 cm reflector around the core. Thus, varying the flat-to-flat distance in the fuel lattice impacted all dimensions in the reactor.

A plot of the reactor is shown in Figure 3-1. The fuel, moderator, reflector and poison are colored red, gray, cyan and blue, respectively. The Figure makes it easy to appreciate the extent to which the overall reactor dimensions change as a function of lattice radius.

As Figure 3-1 shows, increasing the fuel lattice radius results in an increase of moderator and reflector volume. In addition, the fissile inventory increases as well since

the axial dimensions consequently increase to maintain the right circular cylindrical shape. All these factors tend to increase neutron multiplication factor, but after a threshold, the absorption effects in the moderator overcome its moderating effects on neutron flux and have a negative impact on criticality. The purpose of this section of the study is to find that threshold and use it as the optimum lattice radius.

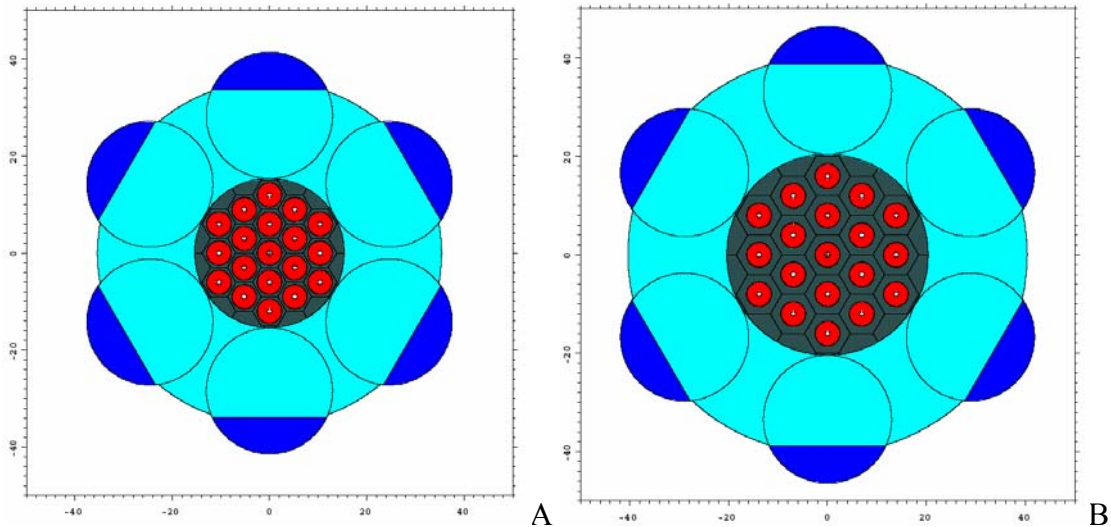


Figure 3-1. Reactor optimization by varying the center-to-flat distance in the fuel lattice. A) reactor layout with 3.0 cm lattice radius. B) reactor layout with 4.0 cm lattice radius.

The data obtained from several runs was collected and plotted in Figure 3-2. The data was also fitted with a third degree polynomial interpolation method, shown in the same Figure. The derivative of the interpolating polynomial was then set equal to zero and solved for its independent variable, thus mathematically maximizing the function. The optimum lattice radius was then found for this system to be 3.6848 cm. After this optimum lattice radius, the k -effective starts to decrease, in spite of the increase of fissile material this entails. Increasing the flat-to-flat distance beyond this point and, consequently, the moderator volume, results in more absorbing material being introduced

in the system. Meanwhile, the increase in moderation is not enough to offset the absorption and result in a net gain in criticality.

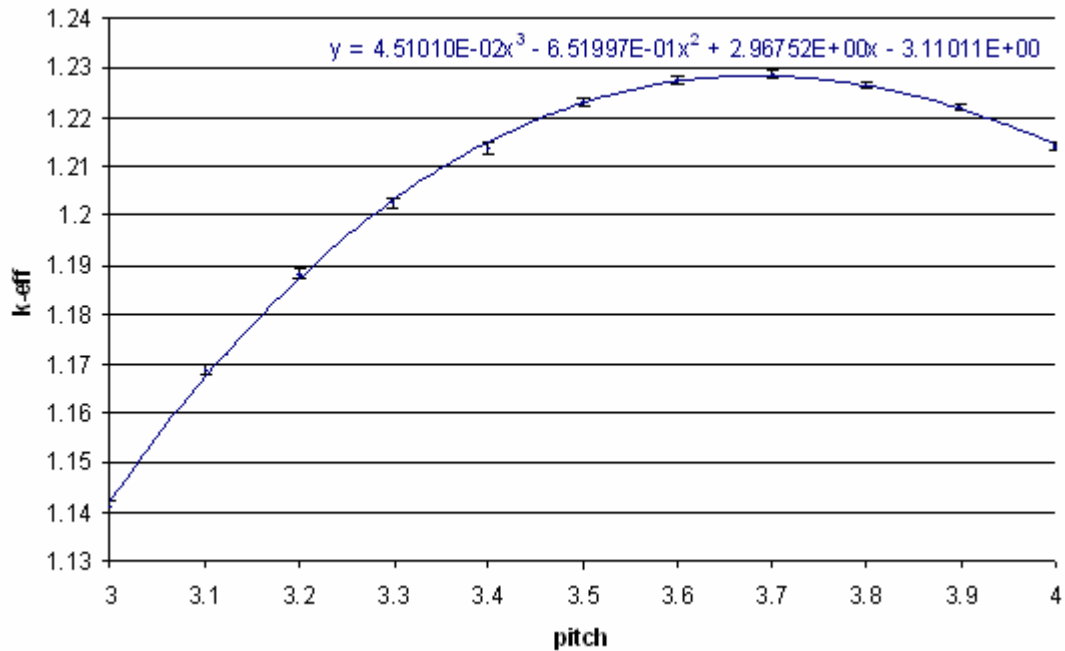


Figure 3-2. Multiplication factor versus lattice radius for the 1.5 g/cc U density reactor.

Once the optimum lattice radius was obtained, the following step was to determine the effect varying levels of Uranium density in the fuel matrix would have on criticality. Such study is explored in the next section.

Uranium Density Optimization and Reactor Temperature Defects

Varying the Uranium density in the fuel matrix will undoubtedly affect the k-effective in the system. It is preferable to have the lowest Uranium density possible, since this will positively impact the thermal conductivity and strength of the fuel matrix material. This is especially important when the fuel matrix is the porous heat exchange medium.

Using the optimum dimensions found in the previous section, several cases were run with varying degrees of Uranium density. The results, which appear in Figure 3-3,

show that the k-effective rises steeply as the density increases before leveling off at higher densities.

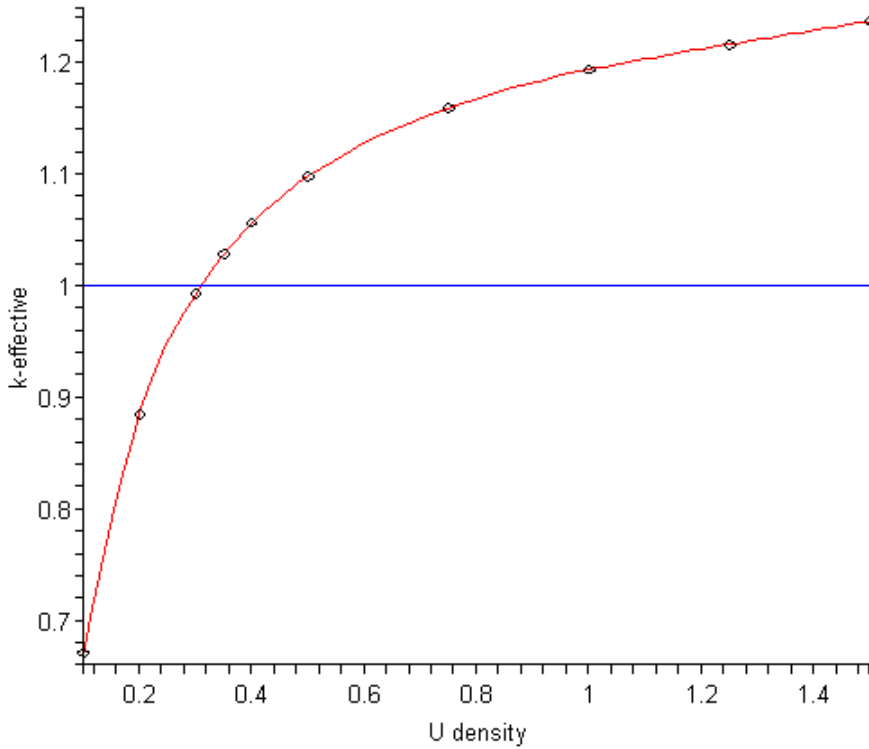


Figure 3-3. Multiplication factor versus Uranium density.

The data shown above was particularly ill-conditioned for even a sixth order polynomial interpolation. As such, we used a cubic spline interpolation method. This generated nine piecewise continuous third degree polynomial functions. These functions are shown in Equation 3-1.

$$k - \text{eff} = \begin{cases} 0.4318662306 + 2.39783769400000012 x - 25.91376942999999986 (x - 0.1)^3 & x < 0.2 \\ 0.5614350778 + 1.62042461100000002 x - 7.77413082911662822 (x - 0.2)^2 + 23.26884714999999992 (x - 0.2)^3 & x < 0.3 \\ 0.7639908420 + 0.7636638600999999980 x - 0.793476683533484550 (x - 0.3)^2 - 5.676010383000000038 (x - 0.3)^3 & x < 0.35 \\ 0.8039688601 + 0.6417461139000000026 x - 1.64487824056583287 (x - 0.35)^2 + 3.639119247000000000 (x - 0.35)^3 & x < 0.4 \\ 0.8551893263 + 0.5045516841999999962 x - 1.09901035420318238 (x - 0.4)^2 + 1.994935123000000008 (x - 0.4)^3 & x < 0.5 \\ 0.9261711665 + 0.3445976669999999996 x - 0.500529817107536745 (x - 0.5)^2 + 0.4277565957000000020 (x - 0.5)^3 & x < 0.75 \\ 1.029117160 + 0.1745371202000000006 x - 0.179712370417624112 (x - 0.75)^2 + 0.1092955589000000006 (x - 0.75)^3 & x < 1 \\ 1.088956148 + 0.1051738522999999996 x - 0.0977407012219669164 (x - 1)^2 + 0.1443411686999999994 (x - 1)^3 & x < 1.25 \\ 1.112360662 + 0.08336747077999999943 x + 0.0105151753054917290 (x - 1.25)^2 - 0.0140202337499999996 (x - 1.25)^3 & \text{otherwise} \end{cases} \quad (3-1)$$

To pick a Uranium density that ensures criticality at beginning of life, the reactor model at 0.35 g/cc was chosen as a first approximation, as this is the first point obtained that results in k-effective greater than one. However, it should be noted that all the runs were performed at operating temperature, with the fuel at 3000°K, the moderator at 800°K, and the reflector at 600°K. To determine startup capability it is necessary to model this system at room temperature and determine if there is a positive reactivity coefficient.

The reactor was modeled with all its components at room temperature so as to ascertain a cold k-effective. Afterwards, the temperatures of the fuel, moderator and reflector were individually increased in separate cases, while leaving the other components at room temperature, to determine their individual reactivity coefficients. These are shown in the last three data columns of Table 3-1.

Table 3-1. Multiplication factor and temperature defects for the fuel, moderator and reflector for reactor with 0.35 gU/cc density.

	Operating temperature	Room temperature	3000 °K fuel	800 °K moderator	600 °K reflector
Eigenvalue	1.02858	0.99428	0.98124	1.0303	1.00607
SD	0.00062	0.00063	0.00062	0.00065	0.00061
$\Delta k/k$ -°K			-4.84485E-06	7.14541E-05	3.86248E-05
			\pm 6.78520E-09	8.49498E-08	4.10477E-08

The data show a negative fuel temperature reactivity defect as well as a positive reactivity defect in the moderator. The latter is over an order of magnitude higher than the fuel temperature defect, and indicates that an increase in moderator temperature, such as that brought about by an abrupt cease in coolant flow, might cause a reactivity excursion. However, the moderator temperature ultimately depends on the fuel temperature, and an increase in the latter would have a negative impact on the multiplication factor. The reflector reactivity defect is also positive, and about half that

of the moderator. The reflector temperature, however, depends on the moderator temperature, which in turn depends on the fuel temperature. In addition, the fuel is separated from the moderator by a gap intended for coolant flow, thus preventing conductive heat transfer between the fuel and moderator. Furthermore, in a loss of coolant scenario, the convective heat transfer to the moderator from the fuel is ceased, limiting a rapid increase in temperature in the moderator.

By lowering the uranium fuel density the fuel to moderator ratio is no longer the same. This results in the system being overmoderated and consequently, an increase in the moderator temperature defect. Thus re-optimizing the system can lower the moderator temperature defect and maximize the k-effective. To do this, the same study presented in Figure 3-2 is repeated for the 0.35 gU/cc core. Results are shown in Figure 3-4.

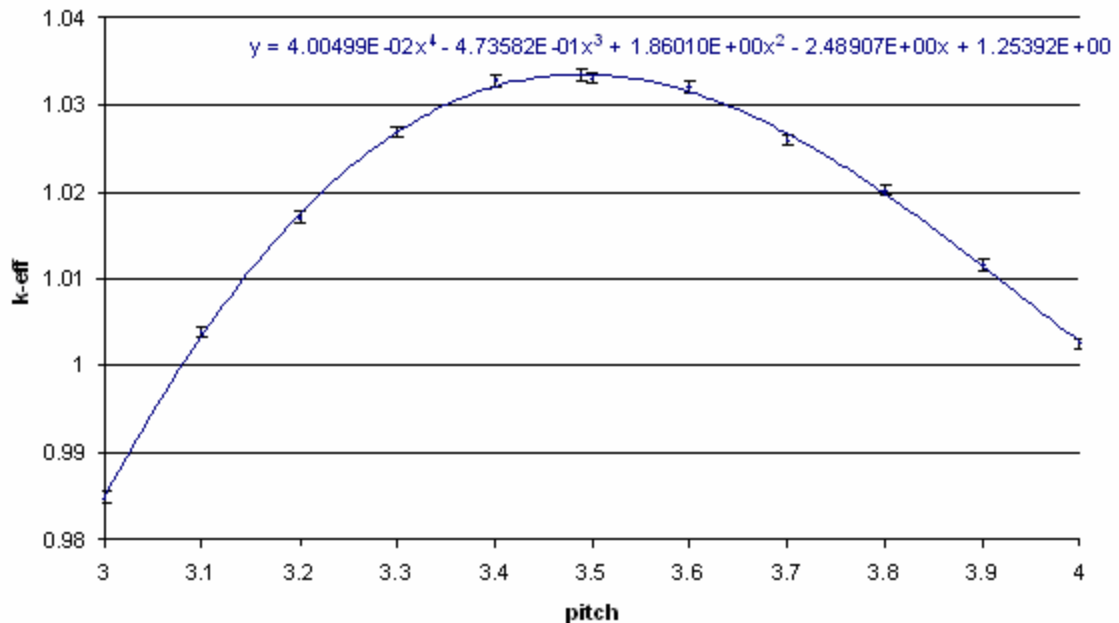


Figure 3-4. Multiplication factor versus lattice radius for the 0.35 gU/cc reactor.

After maximizing the curve presented in Figure 3-4, the optimum lattice radius for the 0.35 g/cm³ fuel is determined to be 3.488 cm. This is 5.3% less than the initial

estimate of 3.685 cm, showing the system as initially modeled was indeed overmoderated. Modeling the system again at the optimum point results in a fuel temperature defect increase of 3.7%, while the moderator temperature defect decreased by 27.3%. Regardless of this improvement, however, the overall temperature defect for the whole system continues to be positive, and the k-effective of the hot core is higher than that of the cold core.

Table 3-2. Re-optimized core multiplication factor and temperature defects for the fuel, moderator and reflector for reactor with 0.35 gU/cc.

	Operating temperature	Room temperature	3000 °K fuel	800 °K moderator	600 °K reflector
Eigenvalue	1.03354	1.00819	0.99448	1.03476	1.01981
SD	0.00065	0.00065	0.00064	0.00067	0.00066
$\Delta k/k$ -°K			-5.02350E-06	5.19806E-05	3.75427E-05
			\pm 6.90287E-09	7.26402E-08	5.65132E-08

Undoubtedly, further reducing the lattice radius will further increase the fuel to moderator ratio, undermoderating the core and decreasing the moderator temperature defect. However, it is important to decide whether an undermoderated core is really desirable considering the potentially catastrophic consequences of water ingress in the core during a launch accident scenario. Nevertheless, the system was again modeled in its cold condition to determine whether the reactivity worth of the hot core compared to the cold core would ever become negative for the case with 0.35 g/cm³ U. For this purpose, the cold system was compared with the system at operating temperatures, with the fuel, moderator and reflector at 3000 °K, 800 °K, and 600 °K respectively. The results are shown in Figure 3-5 as the $\Delta k/k$ that the hot core represents with respect to the cold core.

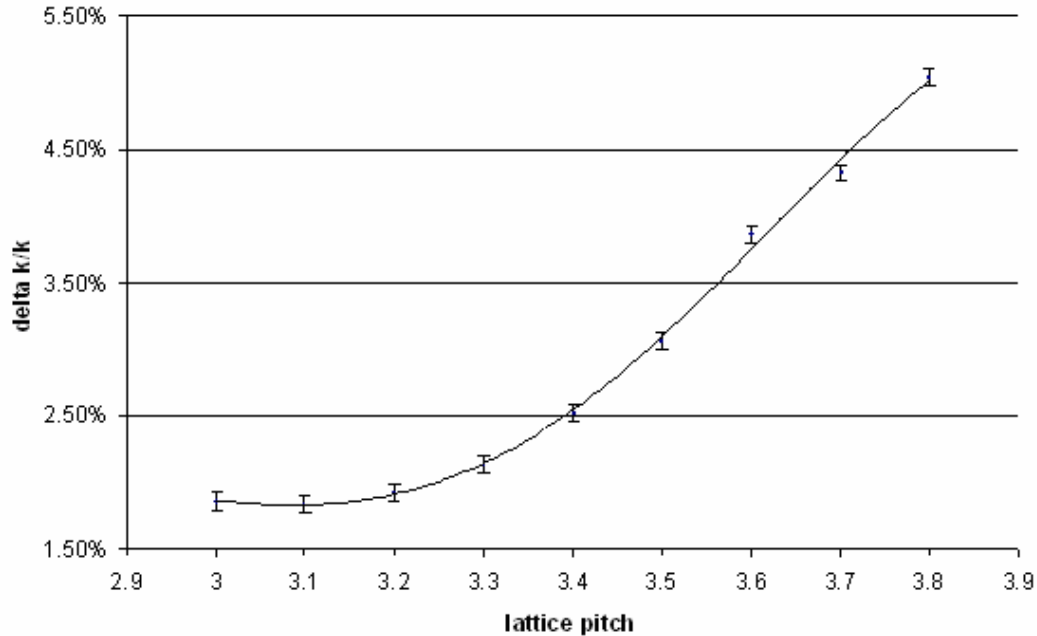


Figure 3-5. Reactivity worth of the reactor at operating temperature.

It is evident from Figure 3-5 that the reactor can never have a negative total reactivity coefficient, at least with fuel at a density of 0.35 gU/cm^3 . There is little doubt, however, that if the uranium density is sufficiently increased the reactor can be undermoderated to a point where a total negative reactivity coefficient for the core can be achieved. Reaching such a high fuel to moderator ratio would also have adverse consequences, such as a more rapid degradation of the fuel matrix and a risk of supercriticality in an accident scenario leading to water ingress. It would appear that the negative consequences of such a design would far outweigh its benefits during reactor operation.

Optimum Reactor Solutions

By using the data presented in Figure 3-3 to interpolate between the curves presented in Figures 3-2 and 3-4, the k -effective can be obtained as a function of lattice radius and uranium density. This relation can help predict the optimum lattice radius as a

function of Uranium density by maximizing the functions generated in the solution space.

The interpolating algorithm used to achieve this is shown in Appendix B.

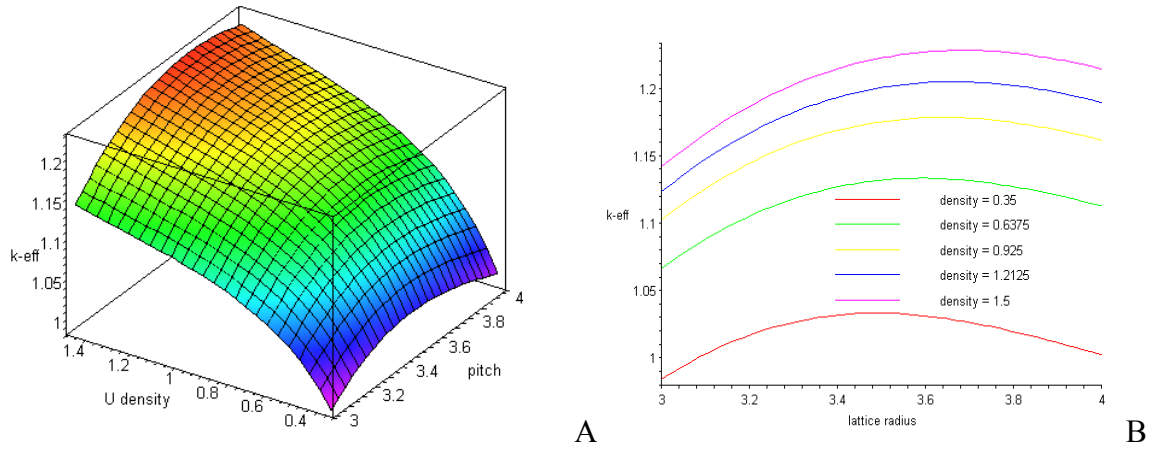


Figure 3-6. Multiplication factor versus Uranium density and lattice radius. A) Continuous interpolated function. B) Discrete interpolated functions at various densities.

As a result of this interpolation, the optimum lattice radius can be found for any uranium density between 0.1 and 1.5. In addition, the k-effective for each of these optimum points can be found from the function plotted in Figure 3-5.

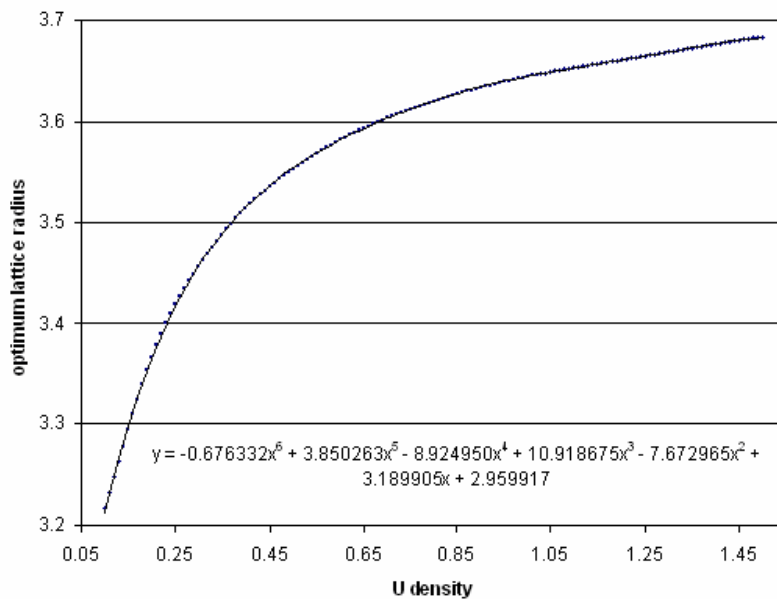


Figure 3-7. Optimized lattice radius for uranium densities between 0.1 gU/cm³ and 1.5 gU/cm³.

The data appears to have a logarithmic behavior as the uranium density is increased. However, this solution is limited to the range of experimental data analyzed and could be different at higher uranium densities. The optimum k-effective corresponding to these points was found by again using the relation plotted in Figure 3-6.

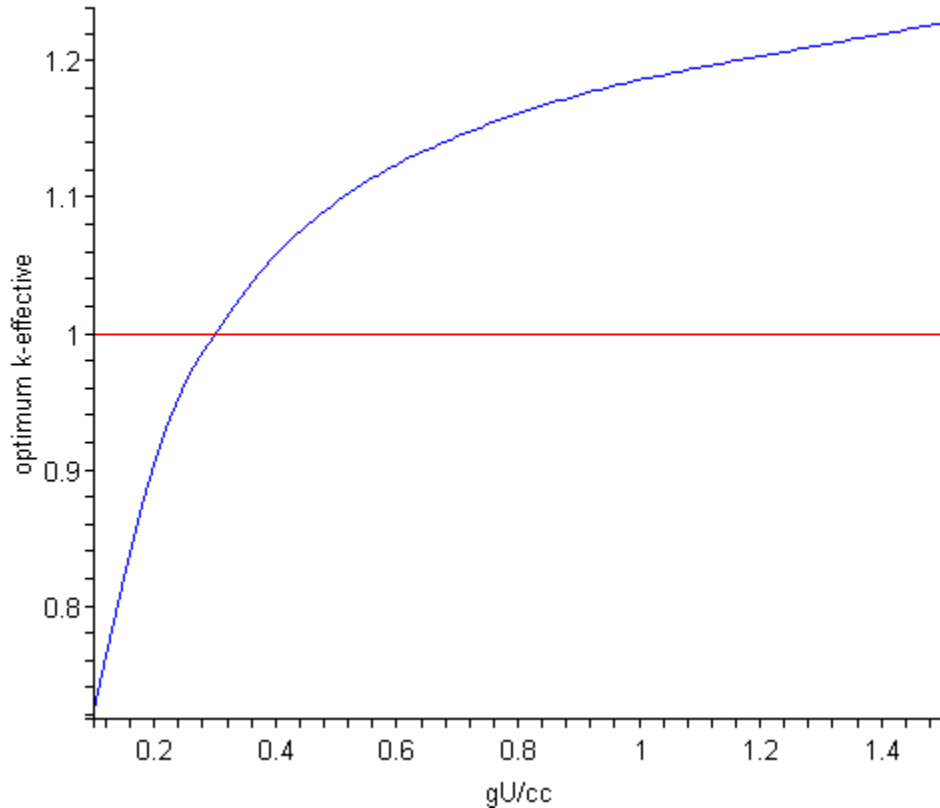


Figure 3-8. Optimized k-effective as a function of uranium density.

This relation is surprisingly similar to the shape encountered in Figure 3-7. Just as the optimum lattice radius appears to reach a limit for higher uranium densities, so does the corresponding k-effective. This behavior also indicates that the system is more sensitive to changes in the moderator when the fuel density is at the lower end of the data, where the optimum k-effective curve is steeper. At higher densities the curve has a lower slope, indicating a lower dependency on changes in the moderator, such as temperature.

Burnup Study

The reactor is designed for two 8-hr burns, one on the approach and one on the return flight to earth. As such, it is necessary that the positive temperature defect be taken into consideration for cold startup of the core. The core of choice will be that which is critical at beginning of life in a cold state, so the cold k-effective is set to one plus three standard deviations (99.7% confidence interval), plus an additional 1% margin. This results in an initial cold k-effective of 1.0130300. Using the previously-obtained temperature defects, this corresponds to a hot k-effective of 1.037876992. According to the mathematical model developed, this corresponds to 0.3577516070 gU/cc and a lattice radius of 3.492698908 cm.

The reactor was modeled with the aforementioned parameters and resulted in a k-effective of 1.03943 ± 0.00096 at operational temperatures (0.15% difference from the model prediction) and 1.01014 ± 0.00094 at shutdown temperature. This means a temperature reactivity worth of 2.90% $\Delta k/k$. The reactivity worth is assumed to remain constant through the burn, since its duration is very brief. Indeed, Figure 3-9 shows the burnup for this reactor during an 8-hour burn within the 95.4% confidence interval. The change in k-effective is very slight, mainly due to the increase in Xe-135 during this period, shown in Figure 3-10. Nonetheless, neither Xenon nor Samarium concentrations reach equilibrium levels in such a brief burn. Samarium inventory reached a total of only 3.66×10^{-5} grams in the core at the end of the brief 70.0 MWd/MTU. The levels of Sm-149 and Pu-239 rose at very similar rates, while the other plutonium isotopes reached a value of only 3.39×10^{-9} grams at the end of cycle.

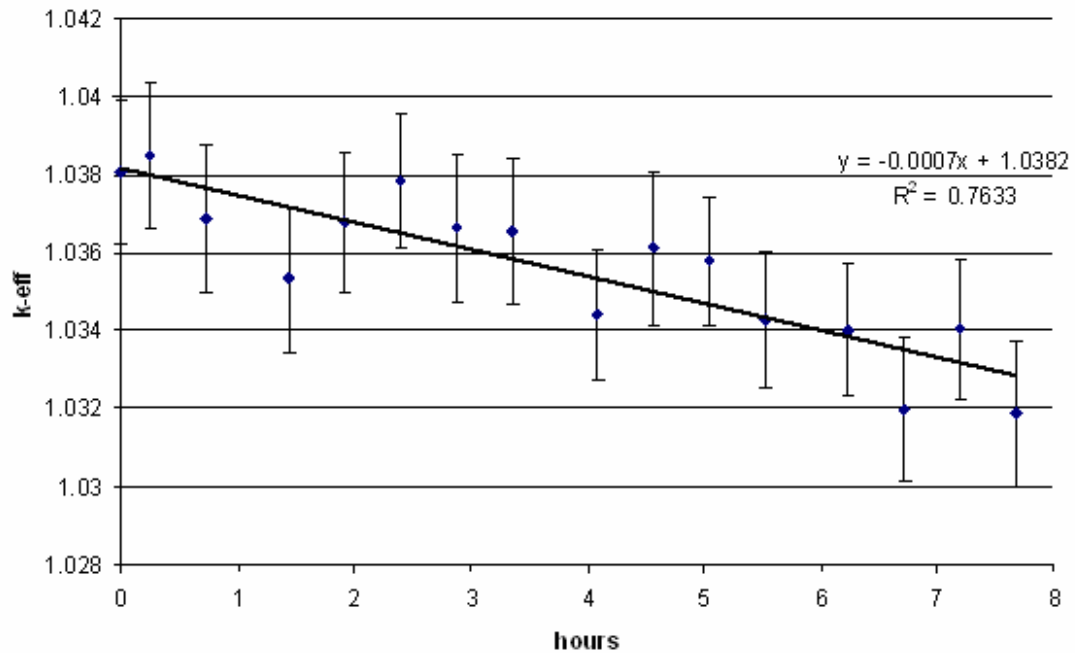


Figure 3-9. Multiplication factor vs. burnup for 8-hr burn at 500 kW thermal power.

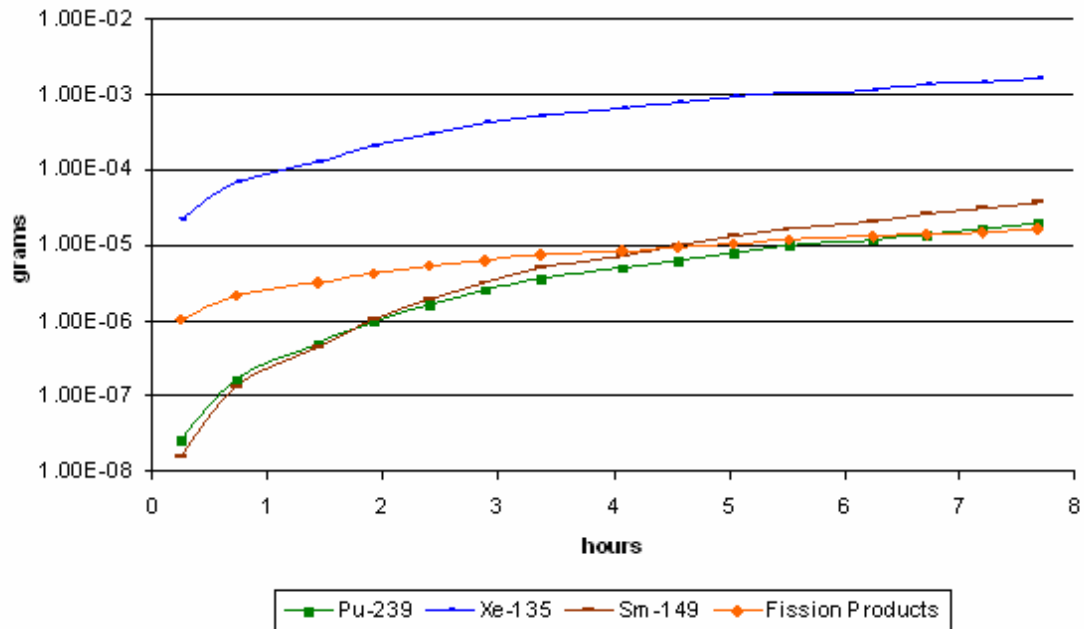


Figure 3-10. Core isotopic inventory for approach burn.

Even though this reactor design is intended for nuclear thermal propulsion, it could also be used for power generation in an electric propulsion system. This can be achieved by coupling the reactor with a closed thermodynamic heat engine, such as a

Brayton cycle, or in a direct energy conversion magneto hydro dynamic system. As such, it would be interesting to see how long the system currently defined could burn for. The reactor was indeed determined to run for ~140 days (30.3 GWd/MTU) before reaching a subcritical state, as shown in Figure 3-11. Undoubtedly, if the mission requires the reactor to run for longer for electrical generation, the uranium content can be increased to reach the demand.

The reactor's extended burn capabilities could be of interest if it were used to power electric ion thrusters instead of its initially intended use as a thermal propulsion system. In a nuclear electric propulsion system the reactor is expected to operate for the entire duration of the mission at lower power levels. Even though the current system is only intended to burn for 8 hours, the positive reactivity defect allows it to burn for much longer than that.

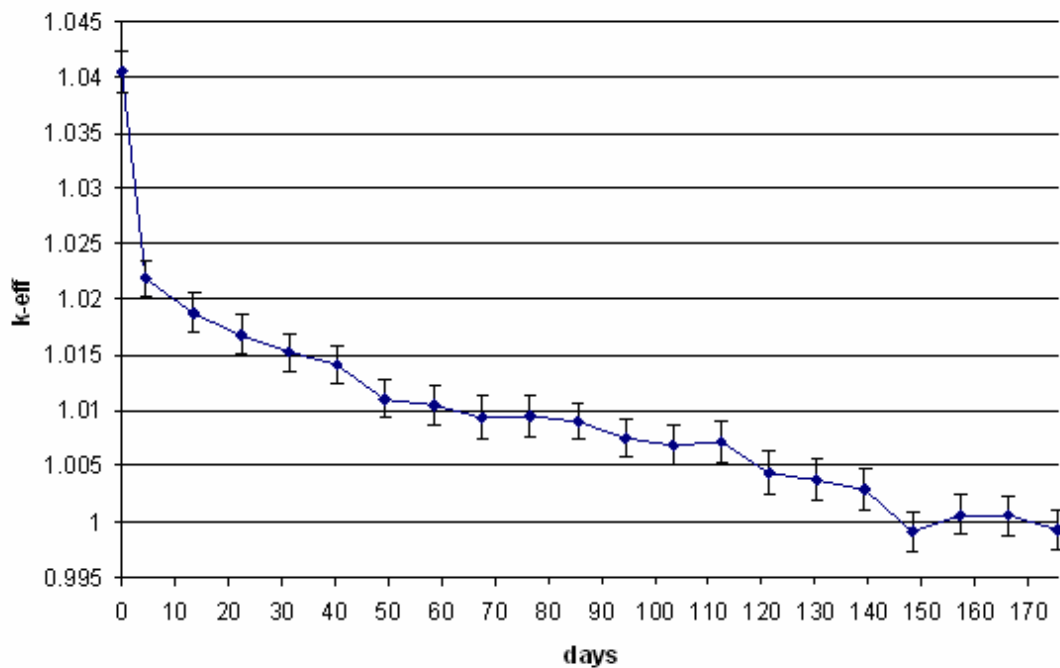


Figure 3-11. Reactor k-effective vs. days in operation.

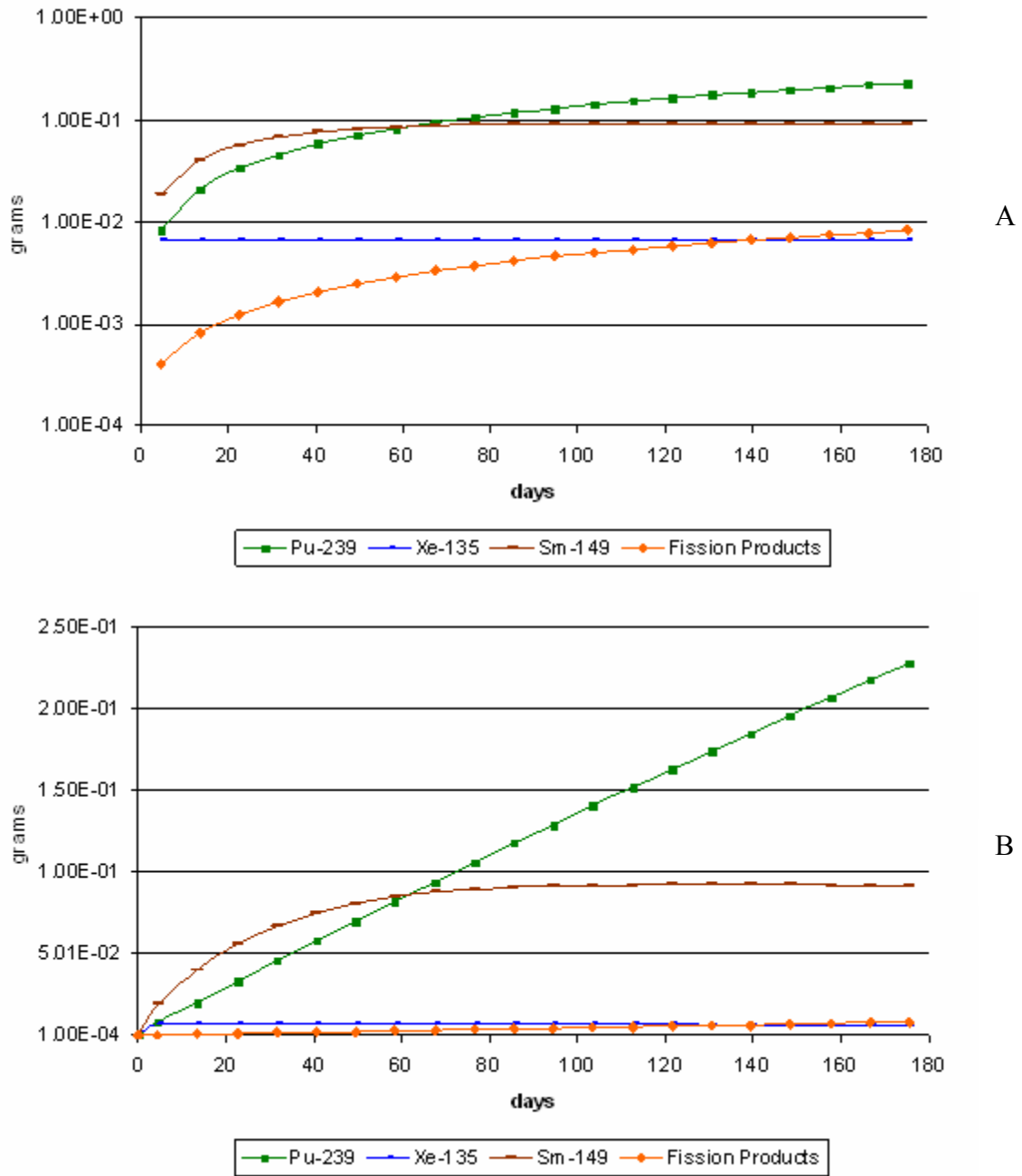


Figure 3-12. Reactor inventory in A) Logarithmic scale and B) linear scale.

As a result of the additional reactivity at operating temperature resulting from a positive reactivity coefficient, the reactor can run for much longer than initially required. During this additional time, there is a steady linear production of Pu-239, easily observed in Figure 3-12 B. Production of xenon and samarium can also be seen in 3-12 A, in a

logarithmic scale. Xenon reaches equilibrium concentration right after startup, while samarium takes roughly two months to achieve equilibrium concentrations.

Control Drum Design and Rotation

Even though control drums have already been selected, it is important to use only the amount of B₄C required. Using more poison will result in the drums having more worth than is necessary, limiting their rotation range. To determine the minimum amount of boron, several cases were modeled with a decreasing size of the boron sliver, as shown in Figure 3-13. Once the results were obtained, the amount of boron selected corresponded to that which would result in a subcritical system at BOL with a two percent safety margin. This corresponds to a k-effective of 0.98. Using cubic spline interpolation shown in equation 3.2 for the data presented in Figure 3-14 results in a desired boron thickness of 0.0366 cm with standard deviation of 0.0007649. The desired value in the 99.7% confidence interval is then 0.0389 cm B₄C.

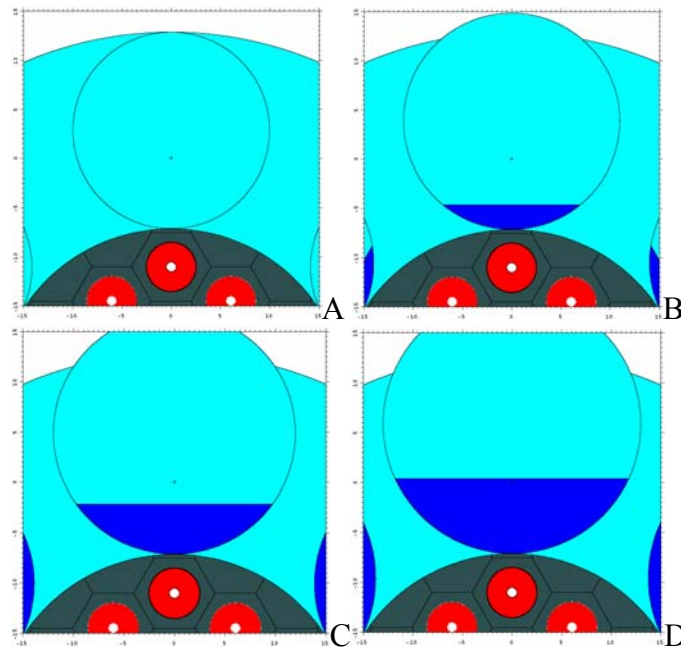


Figure 3-13. Control drums with variable boron carbide thickness of A) 0 cm, B) 1 cm, C) 2 cm and D) 3 cm

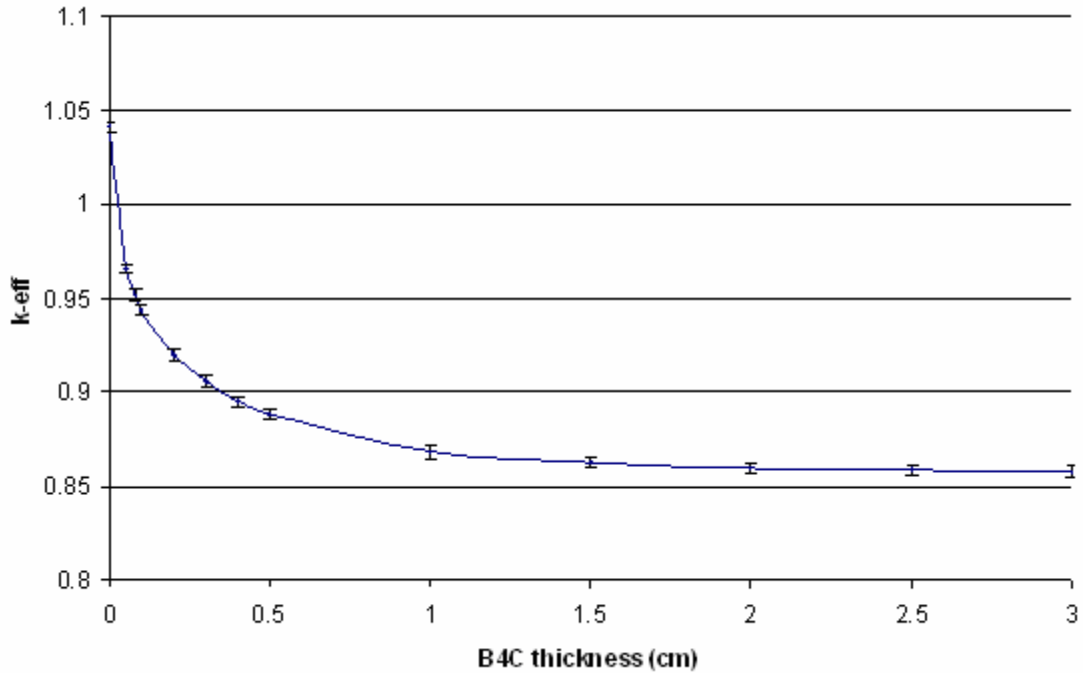


Figure 3-14. Multiplication factor versus B₄C sliver thickness.

$$k - eff = \begin{cases} 1.041120000 - 1.84884654699999996 x + 134.498618999999991 x^3 & x < 0.05 \\ 1.007495345 - 0.840106905299999984 x + 20.1747928454384535 (x - 0.05)^2 - 268.300237299999992 (x - 0.05)^3 & x < 0.08 \\ 0.9795223980 - 0.354029975100000005 x - 3.97222850900509394 (x - 0.08)^2 + 102.436363099999994 (x - 0.08)^3 & x < 0.1 \\ 0.9823495480 - 0.389995479699999980 x + 2.17395327686778872 (x - 0.1)^2 - 6.50998479999999979 (x - 0.1)^3 & x < 0.2 \\ 0.9496808737 - 0.150504368299999997 x + 0.220957837318326022 (x - 0.2)^2 - 0.689141544699999996 (x - 0.2)^3 & x < 0.3 \\ 0.9441461142 - 0.126987047200000008 x + 0.0142153738589064841 (x - 0.3)^2 + 1.07655097800000000 (x - 0.3)^3 & x < 0.4 \\ 0.9313089772 - 0.0918474430500000050 x + 0.337180667246048004 (x - 0.4)^2 - 1.027062367000000009 (x - 0.4)^3 & x < 0.5 \\ 0.9153415903 - 0.0552231806099999986 x + 0.0290619571569012379 (x - 0.5)^2 + 0.00404880814000000040 (x - 0.5)^3 & x < 1 \\ 0.8910146174 - 0.0231246173500000013 x + 0.0351351693742274138 (x - 1)^2 - 0.0234518693500000014 (x - 1)^3 & x < 1.5 \\ 0.8705475250 - 0.00557834998899999976 x - 0.0000426346538109145460 (x - 1.5)^2 + 0.00207866926299999982 (x - 1.5)^3 & x < 2 \\ 0.8677639654 - 0.00406198269499999984 x + 0.00307536924101624398 (x - 2)^2 - 0.00134280770099999992 (x - 2)^3 & x < 2.5 \\ 0.8631942981 - 0.00199371923000000010 x + 0.00106115768974593928 (x - 2.5)^2 - 0.000707438460000000018 (x - 2.5)^3 & otherwise \end{cases} \quad (3.2)$$

After obtaining the boron thickness, the subsequent step was to determine k-effective as a function of control drum rotation. For this purpose the system was simulated at 20° steps from 0° to 180°. The results were plotted and are shown in Figure 3-15 for the 99.7% confidence interval ($\pm 3\sigma$). Since the variation in k-effective was so small in this case, the number of active k-effective cycles was increased to one thousand to decrease uncertainty.

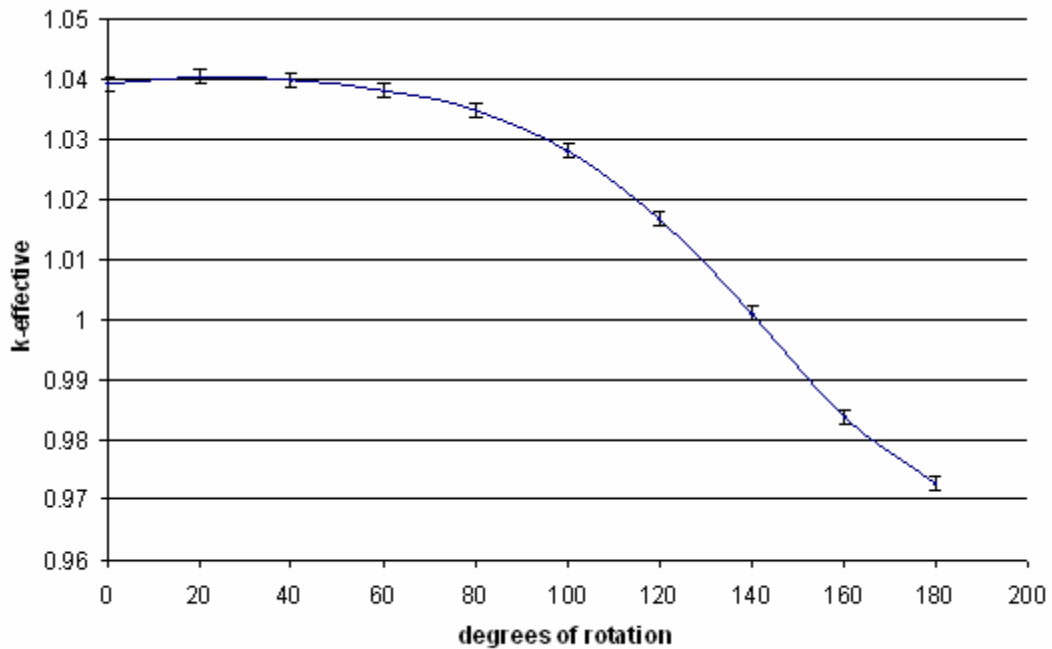


Figure 3-15. Multiplication factor versus control drum rotation.

We used the data in Figure 3-15 to determine the control drum reactivity worth as a function of rotation. This was accomplished by obtaining the difference of each data points with respect to the initial point at 0° rotation. The results (Figure 3-16) were then processed in conjunction with the time-dependent eigenvalues shown in Figure 3-11 to maintain a critical system through the mission duration. This was accomplished by adding k-effective as a function of time to its product with the reactivity worth as a function of rotation. The resulting formulation was then solved for rotation values that satisfied a critical system with time as the independent variable. The resulting inward control drum rotation as a function of days is shown on Figure 3-17. The k-effective for this period of time resulting from applying the calculated control drum rotation is shown in Figure 3-18. Using multiplicative error propagation, the final critical k-effective is estimated to have $\sim 0.1\%$ error.

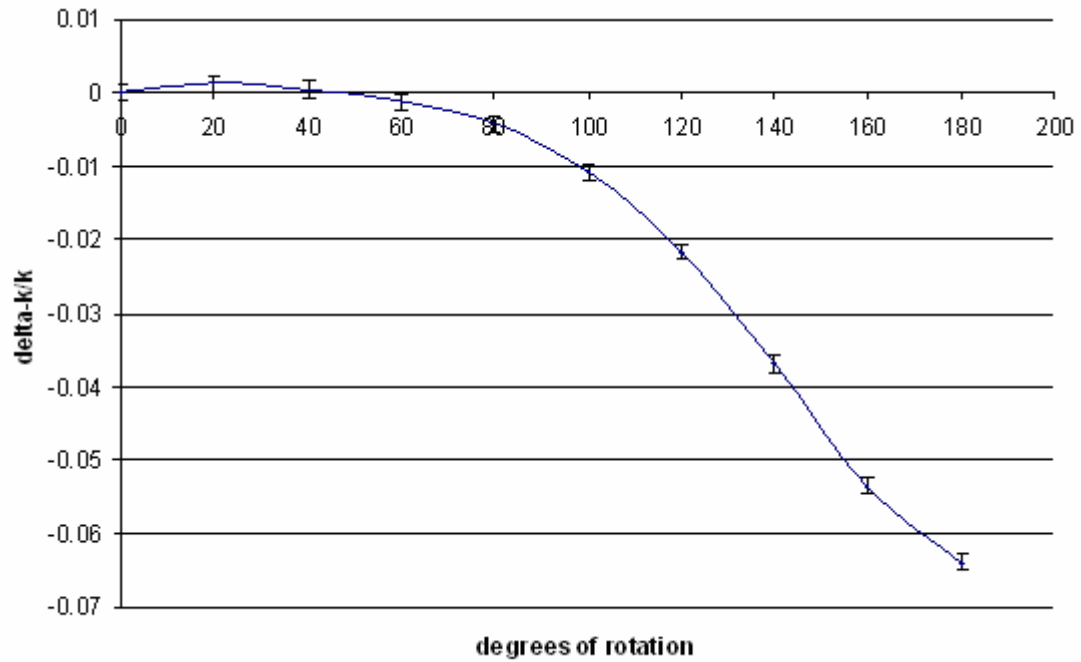


Figure 3-16. Reactivity worth for control drum rotation.

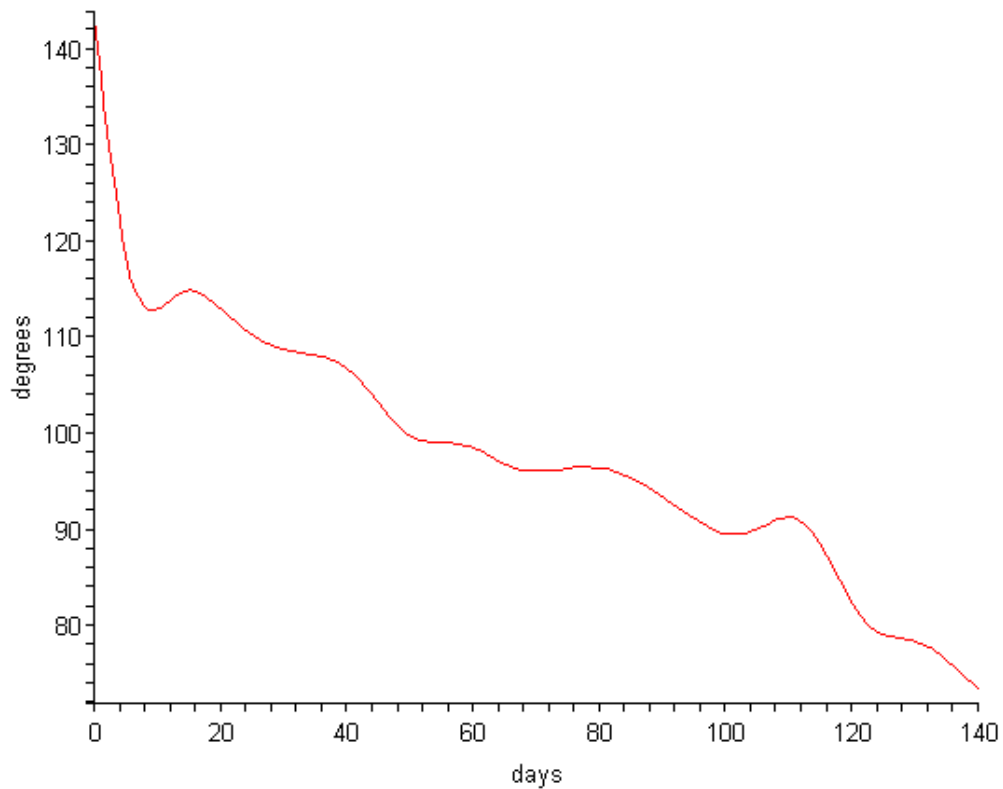


Figure 3-17. Control drum rotation as a function of full power days.

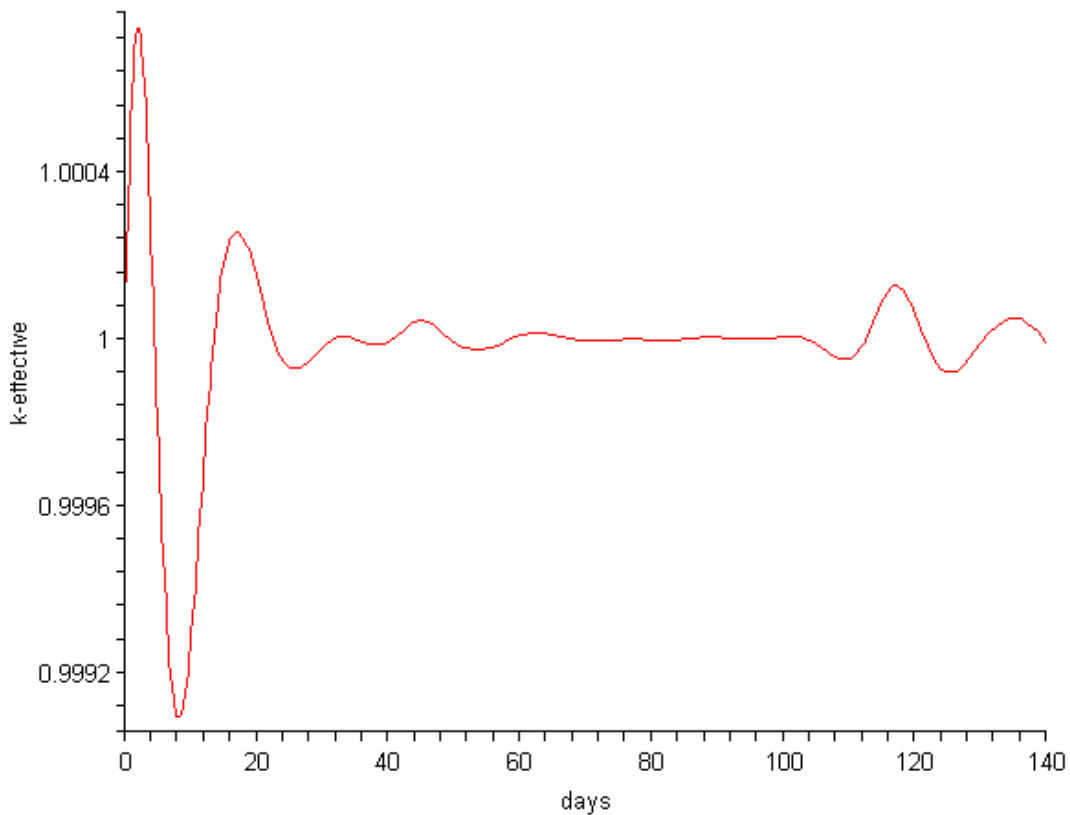


Figure 3-18. Critical k-effective for a 140-day burn.

The statistical error in the calculations causes the mathematical model developed to lose convergence at beginning of life and end of life, as shown in Figure 3-18. However, the model appears to work well during the middle of the burn. The problem stems mainly from insufficient data points and accuracy during modeling of burnup. Due to the limited computational resources available for this work the error unfortunately could not be significantly reduced for this part of the problem.

Alternate Moderator Composition

Besides the reactor design under study, several other variants have been proposed. One of them focuses on replacing the zirconium hydride moderator with yttrium hydride. This section will focus on evaluating the neutronic characteristics of such a design

change. A similar analysis to that performed earlier in this chapter was repeated with the same models. The only difference was that the ZrH_2 moderator was replaced with YH_2 at a density of 5.73 g/cm^3 . The data was obtained by simulating several variants of the system at high uranium density and low uranium density with variable lattice radius, and fitting all data from constant lattice radius and variable density using cubic spline interpolation. A higher amount of cycles were run in this case, bringing the standard deviation to 5×10^{-4} . The absorption cross section for YH_2 is significantly higher than for ZrH_2 , as shown in Figure 3-19, thus, a lower multiplication factor should be expected for any system moderated with YH_2 as opposed to ZrH_2 . Indeed, the results shown in Figures 3-20 and 3-21, illustrate a system with a k-effective field consistently lower than that for the ZrH_2 moderated system.

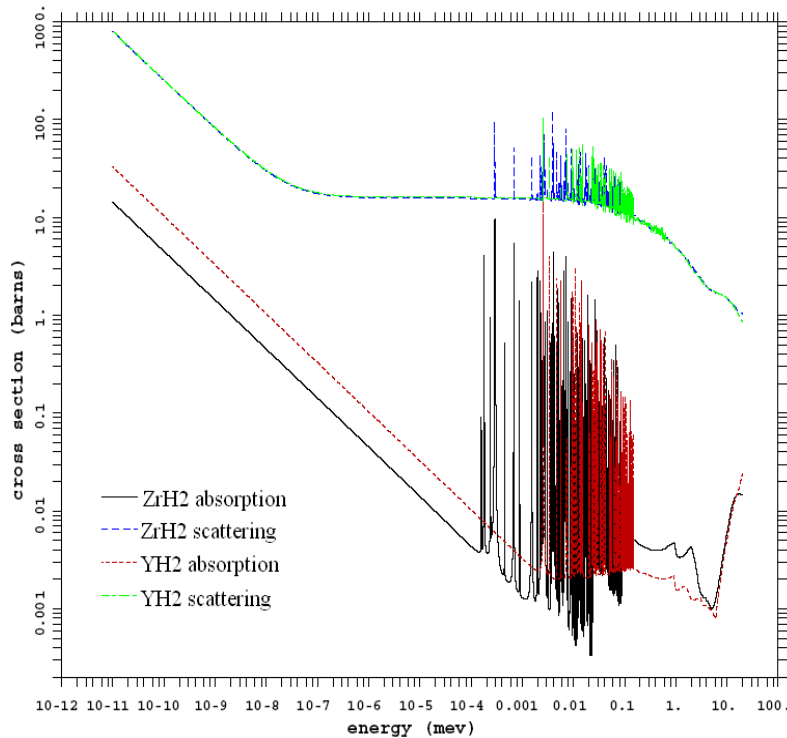


Figure 3-19. Absorption and scattering cross sections for YH_2 and ZrH_2 .

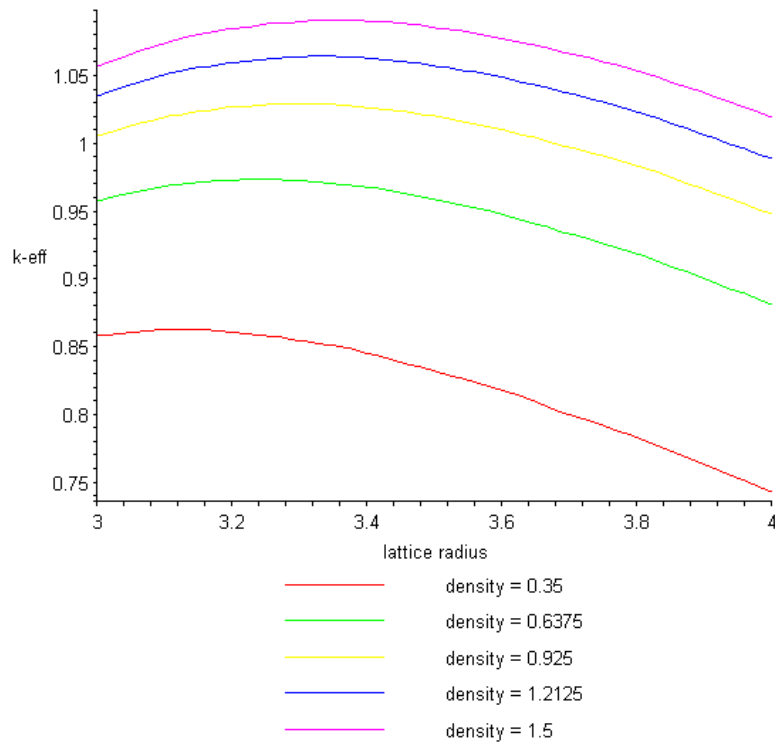


Figure 3-20. Multiplication factor vs. lattice radius for various uranium densities.

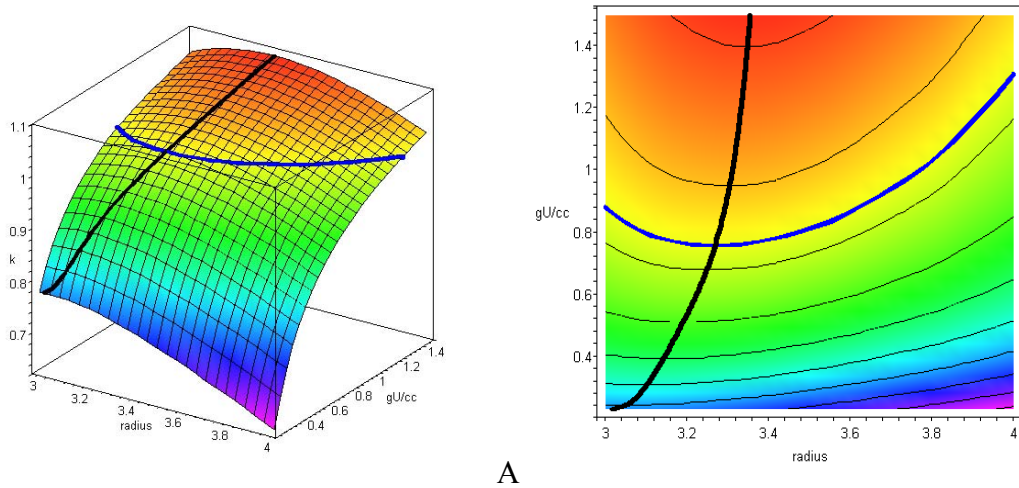


Figure 3-21. Multiplication factor versus lattice radius and uranium density. The thick black curve represents the optimized points and the blue curve represents points where criticality is met. A) Three dimensional view. B) Contour view. The optimized points represented by the black curve were obtained by mathematically maximizing several slices of the k -effective field at constant uranium densities. In addition, the points where the system is critical are represented by the blue curve.

There was a significant and fairly constant difference of $\sim 13\%$ $\Delta k/k$ between the ZrH_2 -moderated system and the YH_2 -moderated system (Figure 3-22). This was expected due to the higher absorption cross-section of YH_2 . However, in spite of the lowered reactivity of the YH_2 -moderated system, the curve of optimized k-effective versus uranium density has a very similar slope to that of the ZrH_2 -moderated system for any value of uranium density.

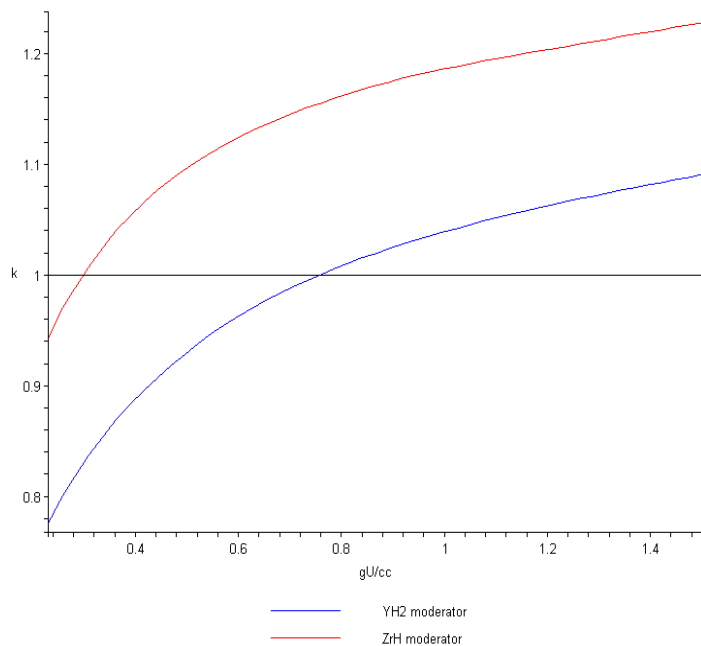


Figure 3-22. Optimized k-effective vs. uranium density for both moderator types.

A critical system was analyzed in order to verify the accuracy of the model in this case. The model predicts 3.268cm pitch and 0.754 gU/cm³ for a critical system, and after modeling such a system on MCNP with the aforementioned parameters, the obtained k-effective was 0.99957 ± 0.00072 . In this case the resulting value for k-eff was statistically the same as the prediction from the mathematical model.

Since yttrium hydride has fewer absorption resonances, and they are present at even higher energies, this material will have a higher positive temperature defect than

zirconium hydride. In fact, the temperature defect for the whole core in this case was 4.589 % $\Delta k/k$.

After reviewing the data presented in the previous three Figures it is evident that the YH_2 moderator carries with it a heavy tax on neutron utilization. As a result, to obtain a critical system, the uranium density necessary in the foam fuel is 153.4% higher in the YH_2 -moderated system than in the ZrH_2 -moderated one. A separate study would need to be conducted to determine if the gains in material properties brought about by yttrium hydride surpass the structural detriment subtended by the fuel matrix by increasing its uranium content.

CHAPTER 4 REACTOR SAFETY AND SHIELDING

This chapter explores the reactor behavior under accident conditions. Before reaching space, the reactor must be launched from a terrestrial facility. If the launch is unsuccessful, the reactor might fall to earth. The concern in this case is to prevent the reactor from reaching criticality no matter what conditions it might encounter when crashed. There are two scenarios that could potentially cause a reactivity increase in the core: falling in sand and falling in water. Sand has been found to be an excellent reflector, as such, a reactor lodged in sand can be assumed to be surrounded by an infinite reflector. In the case of water landing, the water could potentially leak into cavities in the core design for coolant flow, altering the neutron spectrum and physical properties of the system.

Once the reactor is in space and operational, it is important to minimize power peaking. A flat power distribution ensures maximum heat transfer from the fuel by allowing it to be at a higher temperature throughout. In addition, if there is substantial power peaking it can result in fuel melting in certain parts of the core. Because of the nature of the design, a fuel melt scenario would be especially catastrophic, since it would prevent coolant from moving through the fuel. To determine power peaking, this study will examine the thermal flux distribution in the core, since in a thermal system this ultimately dictates where fission occurs.

While the aforementioned provisions are meant to protect the core, it is also important to protect the electronic components in the reactor. For this purpose, a slab of

lithium borohydrate (LiBH_4) was chosen as the shielding material between the reactor and the rest of the ship. To determine the effectiveness of this shielding material, the thermal flux was measured at varying depths in the shield. In addition, $\text{Li}^6\text{B}^{10}\text{H}_4$ was compared with natural LiBH_4 to evaluate the differences between these two materials and determine which would make a better shield.

Infinite Reflector Study

The finalized reactor design was modified to simulate sand immersion. This was performed by adding reflective properties to the outer reactor surfaces, surrounding the reactor by an infinite reflective medium. In addition, the reactor was modeled at room temperature, since it will not be sent at operational temperature. This is important because, due to the positive reactivity coefficient, the multiplication factor in the core is lower when the system is at room temperature.

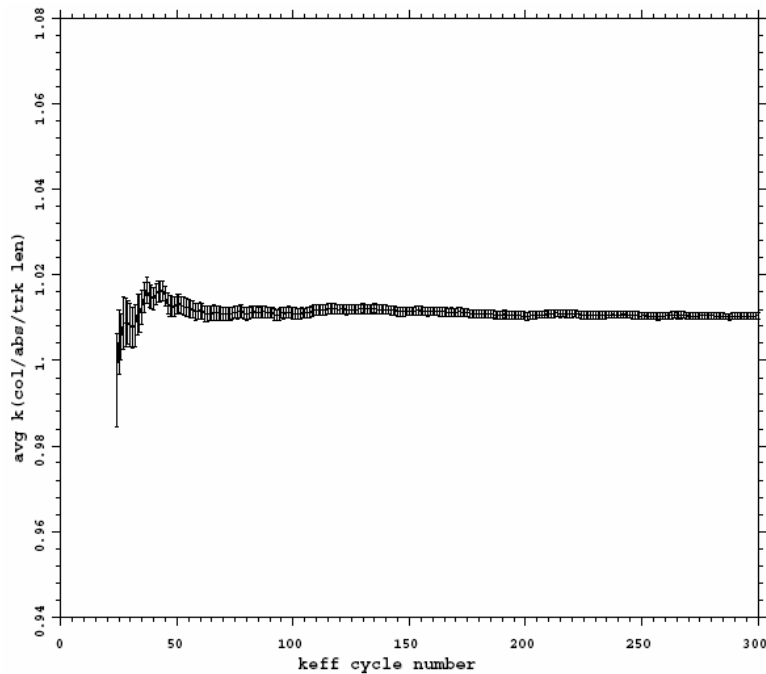


Figure 4-1. Convergence on k-effective for shutdown optimized system in an infinite reflector.

After modeling the reactor with an infinite reflector, it was found that the system would be supercritical under those conditions. The data, shown in Figure 4-1, shows that the final k-effective would be 1.01049 with standard deviation 7.4×10^{-4} . While the designed control drums were sufficient to make the reactor subcritical when surrounded by a non-reentrant surface, such as in space, they were insufficient in keeping the reflected flux from making the system supercritical.

The results confirm that, in case of an unsuccessful launch resulting in sand landing, the reactor would become supercritical, even with the control drums in place. Since the system will be shutdown, no coolant will be flowing through the core. In addition to the heat generated from fission, the lack of cooling would further contribute to the increase in temperature in the fuel and the system as a whole. Because of the positive reactivity coefficient in the core, this will result in a further increase in k-effective, resulting in the temperature increasing even more. As a direct consequence of the very high temperatures likely to be reached in the system the fuel will melt and core materials and structural support will suffer severe degradation. The core will collapse and its contents will escape into the environment. Fortunately, this would happen with a clean core, so iodine-131, strontium-90, cesium-137 and other fission products would have no inventory in the core at the beginning of the accident. However, these fission products would be produced and released as long as the core stays critical or supercritical.

These results are undoubtedly unacceptable, and could be remediated in several manners. One such methods might include enlarging the thickness of the boron sliver in the control drums, since according to Figure 3-14, the maximum reactivity worth

attainable with this method is $0.17643 \Delta k/k$. However, doing this would limit the range of motion of the drums once the system is in operation, limiting the resolution with which control is maintained.

Water Immersion Study

To simulate the water landing scenario, the reactor was modeled with water in the inner and outer radial coolant flow gaps, as well as filling up the pores in the foam fuel. In addition, the reactor is assumed to be fully submerged in a body of water, and as such it was modeled as being surrounded by a water sphere with a ten meter radius. The number density of materials comprising the fuel cylinders are shown in table 4-1. The water filling the inner and outer coolant gaps was modeled at 1 g/cm^3 .

Table 4-1. Elemental composition of water-fuel mixture

<u>Element</u>	<u>Number Density (b-cm)⁻¹</u>
U-235	8.88800E-04
U-238	2.75000E-05
Zr	2.92010E-02
Nb	9.73370E-03
C	3.98509E-02
H	3.34367E-02
O	1.67183E-02

In the event of a water landing, the core and foam fuel will be filled with water, and in addition the sphere surrounding the reactor will contribute to additional moderation in the medium. Several options were explored to maintain the core subcritical in this instance. These included the insertion of boron carbide control plugs in the central coolant channels in the fuel elements. One variant used a control plug in the central fuel element, while the other used plugs in all fuel elements. In addition, the reactor was also surrounded by varying thicknesses of B_4C foil to prevent the reflected

flux from contributing to k-effective. The data from these runs is presented in table 4-2.

All cases had standard deviation in the order of 8×10^{-4} .

Table 4-2. Multiplication factor for the system surrounded by varying thicknesses of boron carbide foil, with a boron carbide plug in the central fuel element and in all fuel elements.

Foil thickness (mm)	0	1	2	3	4	5
No plugs	1.227	1.22467	1.22393	1.22328	1.22425	1.22402
Central plug only	1.2045	1.20023	1.20094	1.20151	1.20243	1.2012
All plugs	1.03074	1.00795	1.00639	1.00881	1.00863	1.00907

Foil thickness (mm)	10	20	30	40	50
No plugs	1.22518	1.2248	1.22566	1.22397	1.22287
Central plug only	1.20115	1.20205	1.20066	1.2017	1.19906
All plugs	1.00777	1.00907	1.00832	1.00945	1.00741

In none of the cases explored was the system kept subcritical under a water landing accident scenario. The fact that adding a thicker layer of boron carbide around the outer surface of the reactor was unsuccessful is of special interest. This means that most of the contribution to excess reactivity originates from the water inside the reactor. Inserting control plugs in the central region of all fuel elements did bring k-effective down a bit, but the system was still supercritical. This is attributed to increased moderation and subsequent spectral shift in the water-filled foam, outer coolant cavities, and ZrH_2 moderator. The magnitude of the thermal flux in this area is increased due to the fact that they are contiguous. Indeed, Figure 4-2 shows that in a system with no outer foil and all nineteen control plugs, the thermal flux, responsible for 88.31% of fissions, rises rapidly from the center of each fuel element. In the intermediate spectrum from 0.625 eV to 100 keV, responsible for 10.42% of fissions, this behavior is again observed, with the flux being depressed only at the center.

It would seem that if the thermal flux could be depressed on the outer gaps of the fuel elements, this problem could be corrected. Placing a neutron poison at these locations should prove an effective way to prevent criticality, and indeed it does. Figure 4-3 shows the flux distribution in the reactor after filling the peripheral gaps in the fuel elements with B_4C .

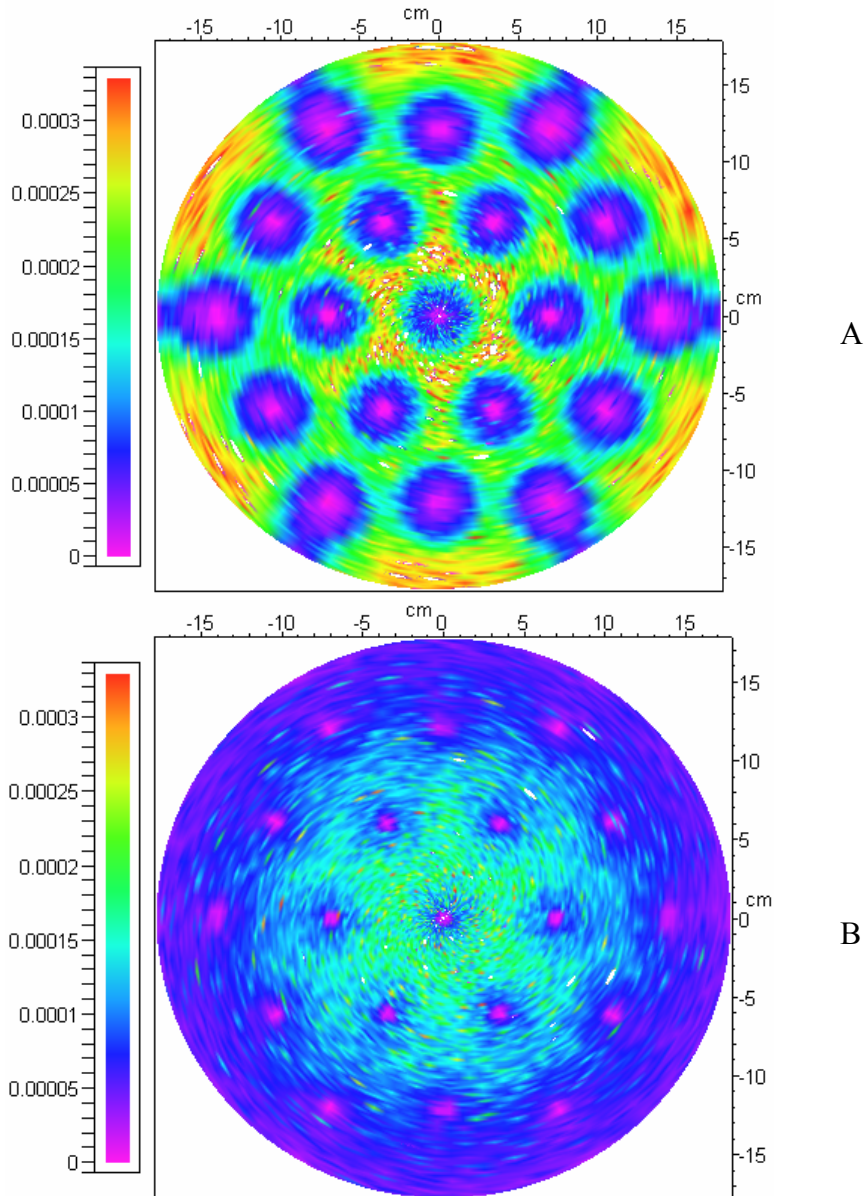


Figure 4-2. Neutron flux in the reactor with inner control plugs in all fuel elements, normalized to particle histories. A) Energy range 0 eV to 0.625 eV (88.31% of fissions). B) Energy range 0.625 eV to 100 keV (10.42% of fissions).

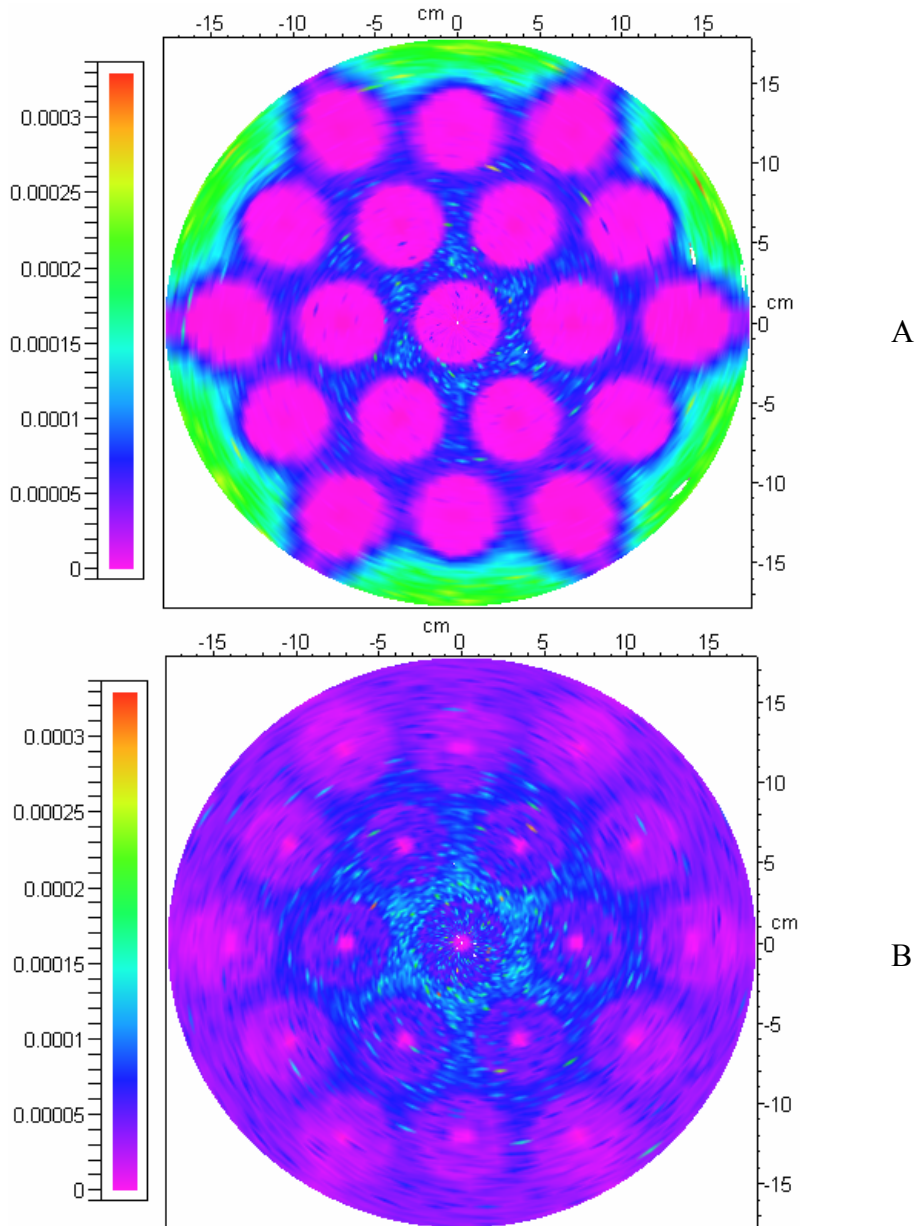


Figure 4-3. Neutron flux in the reactor with inner control plugs and shells in all fuel elements, normalized to particle histories. A) Energy range 0 eV to 0.625 eV (49.14% of fissions). B) Energy range 0.625 eV to 100 keV (41.64% of fissions).

Placing control shells surrounding the control plugs in each fuel element clearly depresses the thermal flux in the fuel elements. As evidenced by Figure 4-3 A, the thermal flux is consistently depressed in the fuel by use of this system. In addition, the intermediate flux, responsible for 42% of fissions in this case, is also depressed on the

periphery of the fuel elements, as evidenced by Figure 4-3 B. This results in the k -effective for this system being 0.13628 with standard deviation 3.2×10^{-4} , a value 86.8% lower than that resulting from the use of central control plugs alone. This proves that the reactor can safely crash in a body of water and stay subcritical if equipped with central control plugs and peripheral control shells during launch. In addition, the use of a control foil surrounding the reactor is not necessary. Since this measure prevents criticality in case of water immersion, it will also maintain the system subcritical in case of sand immersion, since excess criticality in that case is only a fraction of that observed in water immersion.

The use of multiple control plugs and shells will require additional mechanical complexity in the system. To eject them, the nozzle will need to detach from the reactor. As a result of this requirement, an interchangeable mechanism could be developed to swap the nozzle with the hot leg of a heat engine or MHD energy conversion unit as required. This results in a more versatile system, as it can be used for thermal propulsion, electric propulsion, and auxiliary power generation.

Operational Reactor Flux

To determine the reactor flux while in operation, the reactor was modeled with the control drums rotated outwards and with no safety plugs or shells. In this case, 91.4% of fissions were caused by thermal neutrons from 0 eV to 0.625 eV and thus, the thermal flux provides an excellent indicator of power distribution in the core. The thermal flux distribution across the core is shown in Figure 4-4. The plot qualitatively shows very little difference in the thermal flux between the fuel elements. This indicates that power peaking is not very pronounced.

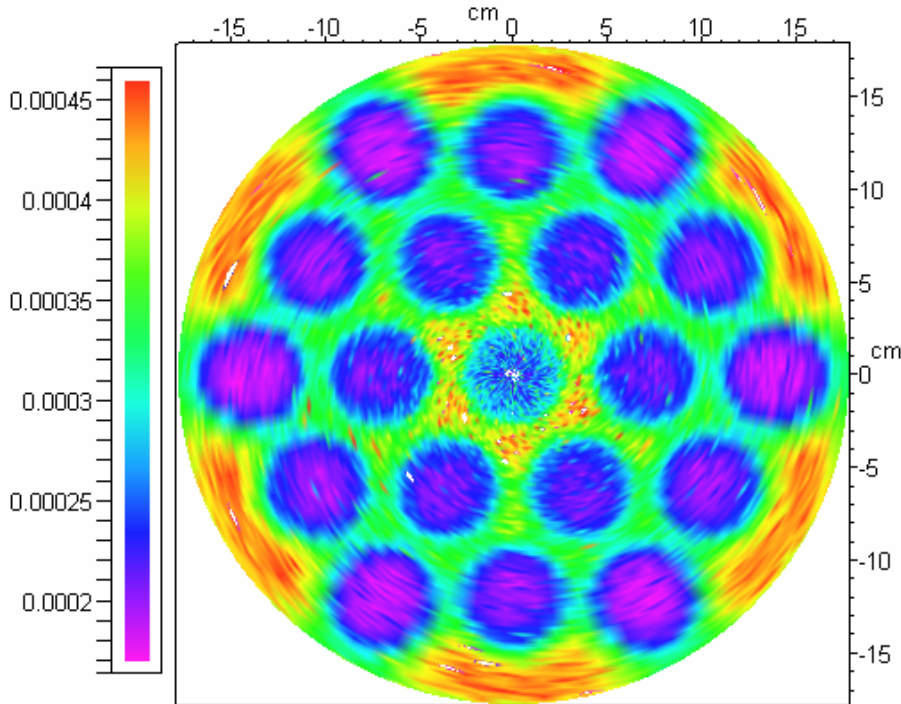


Figure 4-4. Thermal neutron flux in the reactor core from 0 to 0.625 eV

The thermal flux can be processed further to give a better indication of power peaking through the fuel. By normalizing the flux in the areas of the core occupied by the fuel, the power peaking values for the fuel, presented in Figure 4-5 are obtained. This data suggests that the fuel has a fairly flat power distribution, slightly higher towards the center of the reactor. However, the thermal flux (and therefore power) is consistently higher on the outer periphery of each fuel element, while it is depressed in the center of the fuel element. This feature appears to be shared among all fuel elements regardless of location in the core. The inward directed coolant flow should offset this effect, since the cold hydrogen first comes in contact with the outer periphery of the fuel elements, where the power is higher. As a result, coolant flow should drive the temperature profile towards an isothermal shape in the fuel.

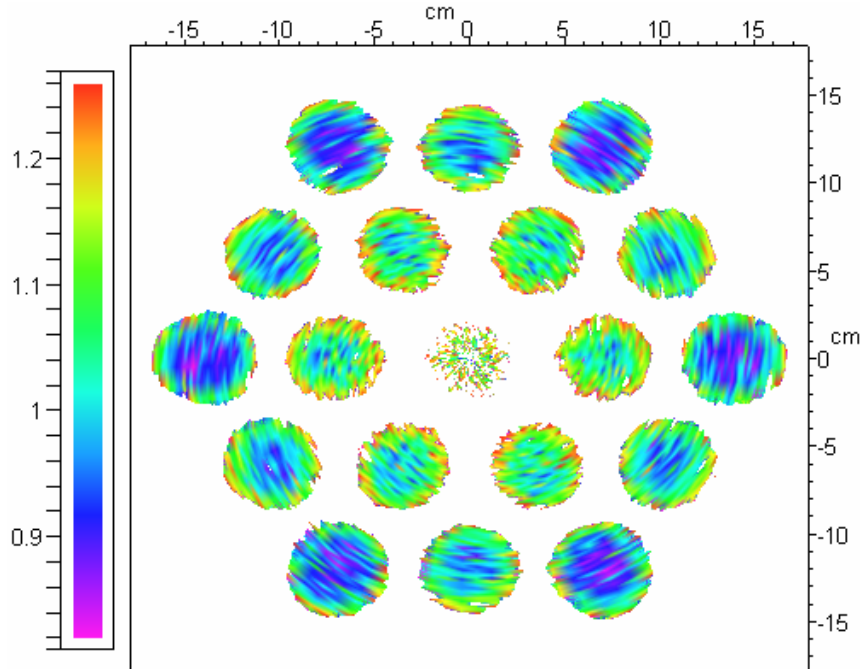


Figure 4-5. Power peaking factors in the fuel.

Thermal flux levels are understandably higher in the operational core than they were in the shutdown core with all safety devices inserted. In addition thermal flux is responsible for 91.4% of fissions in the system, facilitating control due to the higher contributions of delayed neutrons.

Reactor Shielding

A space mission not only requires propulsion, but also an array of scientific instrumentation and possibly a crew. Proper reactor shielding must be used to keep components and astronauts from being damaged by neutron radiation. This section evaluates the use of a 20-cm slab of lithium borohydride (LiBH_4) as a shielding material. Natural LiBH_4 was compared with $\text{Li}^6\text{B}^{10}\text{H}_4$ to determine to what extent shielding can be improved with the alternate isotopic composition.

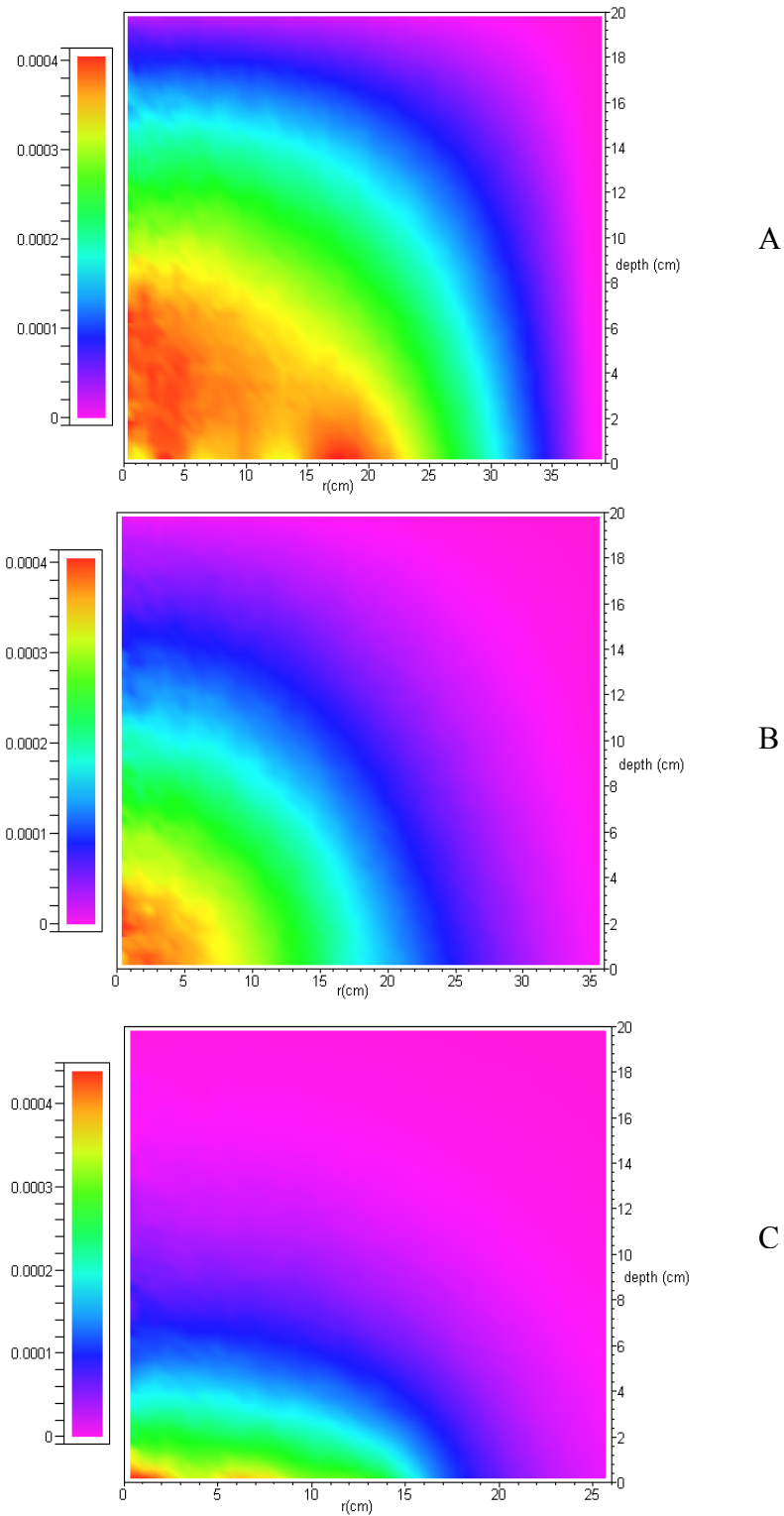


Figure 4-6. Normalized neutron flux in axial BeO reflector. A) Thermal flux from 0 eV to 0.625 eV. B) Intermediate flux from 0.625 eV to 100 keV. C) Fast flux from 100 keV to 20 MeV.

In addition to the LiBH_4 slab, the reactor's BeO reflector does a significant amount of shielding by itself. In keeping neutrons in the reactor, a great deal of leakage is prevented as well. The normalized flux distribution in the BeO slab adjacent to the LiBH_4 shield is shown in Figure 4-6. The plot shows a substantial reduction in all spectrums. The thermal flux is reduced by 92.2% across the reflector, while the intermediate and fast flux are reduced by 94.7% and 98.5% respectively. Clearly, the system can be thought of as having two shields, the first of which being the reflector.

The use of a LiBH_4 shield brings about additional attenuation, as shown in Figure 4-7. A significantly larger attenuation in the intermediate energy group results in the $\text{Li}^6\text{B}^{10}\text{H}_4$ shield than in the natural LiBH_4 counterpart. There is no statistically significant difference between the two materials in the fast group. The thermal group attenuates very quickly in the slab, with the $\text{Li}^6\text{B}^{10}\text{H}_4$ being more effective at this.

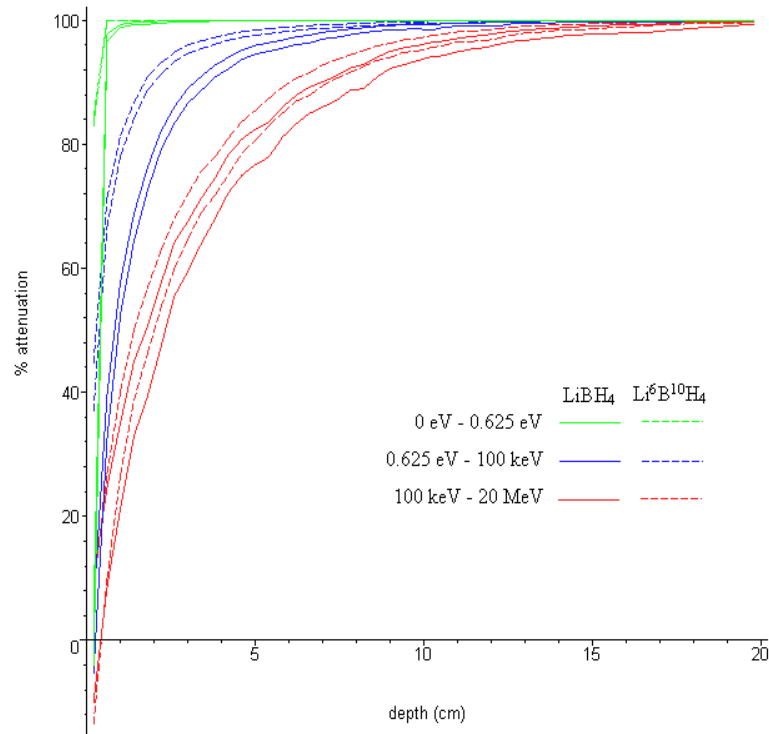


Figure 4-7. Attenuation percent across the LiBH_4 shield, \pm standard error corresponding to one standard deviation.

The combination of the BeO reflector and an additional $\text{Li}^6\text{B}^{10}\text{H}_4$ or LiBH_4 slab proves to be a very effective way to attenuate the neutron flux to the rest of the vehicle. The 20-cm thick $\text{Li}^6\text{B}^{10}\text{H}_4$ shield provides, at the lower limit of the error margin, 99.97663639 %, and 99.60847405 % attenuation the intermediate and fast spectrums respectively. Natural LiBH_4 , on the other hand, results in 99.91972275 % and 99.18713220 % attenuation in the intermediate and fast spectrums respectively. The thermal flux attenuation in the shield was not as simple to obtain, since many of the tallies were zero into the slab.

By using the difference in flux in the first 2 cm of the slab, a linear attenuation coefficient was derived and used to approximate the thermal flux attenuation through the slab. Using the standard error corresponding to one standard deviation, this resulted in a fraction of transmitted radiation in the range of $8.819148271 \cdot 10^{-86}$ to $1.735657896 \cdot 10^{-79}$ for the natural LiBH_4 and $1.239948923 \cdot 10^{-116}$ to $2.963058401 \cdot 10^{-103}$ for the $\text{Li}^6\text{B}^{10}\text{H}_4$ shield at 20 cm thickness. These results indicate that essentially no thermal neutrons can get through the slab, since the highest conceivable neutron flux would be in the order of 10^{16} n/cm²-s.

Even though $\text{Li}^6\text{B}^{10}\text{H}_4$ proves to be a better shield than natural LiBH_4 , the latter still proves to be quite a formidable shield at 20 cm thickness. When attenuation from the BeO reflector is taken into account, the total fraction of neutrons that transverse both the reflector and LiBH_4 shield, at the most conservative limit of the error margin, is $1.405339639 \cdot 10^{-82}$, 0.00004529993750, and 0.0001337806510, for the thermal, intermediate and fast groups respectively. For the $\text{Li}^6\text{B}^{10}\text{H}_4$ shield, these values were $2.399149874 \cdot 10^{-104}$, 0.00001318393533, and 0.00006443679585 for the thermal,

intermediate and fast energy groups, respectively. This data suggests that, using the ratio of their multiplicative spectral attenuation aggregates, $\text{Li}^6\text{B}^{10}\text{H}_4$ is 97.5% more effective as a shielding material than its natural counterpart. In spite of this, sufficient attenuation can be obtained by the use of either material. In addition, a 20 cm slab may not be necessary. The thickness of the slab can be significantly less, reducing the payload mass. Ultimately, only the required radiation limit would dictate the amount of shielding required.

CHAPTER 5 SUMMARY AND CONCLUSIONS

Summary of Results

The main goal of this work was to develop a model of the neutronic behavior of the foam fuel reactor and evaluate it as a feasible candidate for a space power and propulsion system. The results presented in chapter 3 showed that the system would work from a neutronic point of view. In addition, it was shown that the reactor can have enough excess criticality to run for an extended period of time.

Chapter 4 evaluated different accident scenarios, and recommendations were made to include axial and central control elements to be used during launch to prevent criticality in case of failure. However, this implied that the nozzle or hot leg needs to be detached from the system to eject the safety controls prior to reactor startup. This adds additional mechanical complexity to the system, and this is typically unwanted in space systems.

There were some troubling results suggesting that the system would have a positive reactivity coefficient regardless of how it is designed, as long as the moderating materials under evaluation are used. This is due to the ZrH_2 not having absorption resonances any lower than 100 eV. Doppler broadening effects are comparatively small in this case because 91.4% of fissions are caused by neutrons with energy less than 0.623 eV. Thus, increases in moderator temperature will have mainly a $1/v$ effect, decreasing neutron absorptions in the moderator. This problem is exacerbated through the use of YH_2 , since this material has even fewer absorption resonances, and those that are present

appear at energies greater than 2 keV. As a result, when YH₂ is used as the moderator the system has a 58 % higher temperature defect.

The positive reactivity in the core could be counteracted by a feedback mechanism controlling control drum rotation based on moderator temperature monitoring and/or thermal flux levels. With advanced computers available nowadays, this algorithm should not be a big technical challenge. In addition, the reactor operates on the thermal spectrum, making control even easier thanks to delayed neutrons.

Data Summary and Delivery as Maplets

The data obtained for reactor parameter correlations in Chapter 3 was compiled and summarized as maplets, included in this document. Two maplets were compiled, one for the ZrH₂ moderated reactor and one for the YH₂ moderated reactor, accessible as objects 5-1 and 5-2, respectively. In each case, the user is first given the choice to select the desired input in a dialog shown in Figure 5-1 A. Once selected, the dialog disappears and the user is prompted to input the value of the desired parameter, as shown in Figure 5-1 B. Pressing the “Evaluate” button or return key then returns the other corresponding parameters at the optimal point according to the mathematical model. In addition, the “Plot” button plots the location in the relevant section of the data where this point falls. The black curve corresponds to optimized parameters, and the khaki curve corresponds to the k-effective at the point. In addition, the “Help” button displays an information window showing the user the range of values for the system. There are error messages built in to the maplet that prevent it from crashing if the user inputs values out of the data range. The other options are “Clear” and “Exit”, which perform the functions implied.

The maplets were created using Maple 9.5, but might also work with other versions of Maple with perhaps limited functionality. They can be executed by double-clicking

the files on a windows PC with Maple installed. Maple's maplet viewer should automatically open the files, appearing to the user as an executable application.

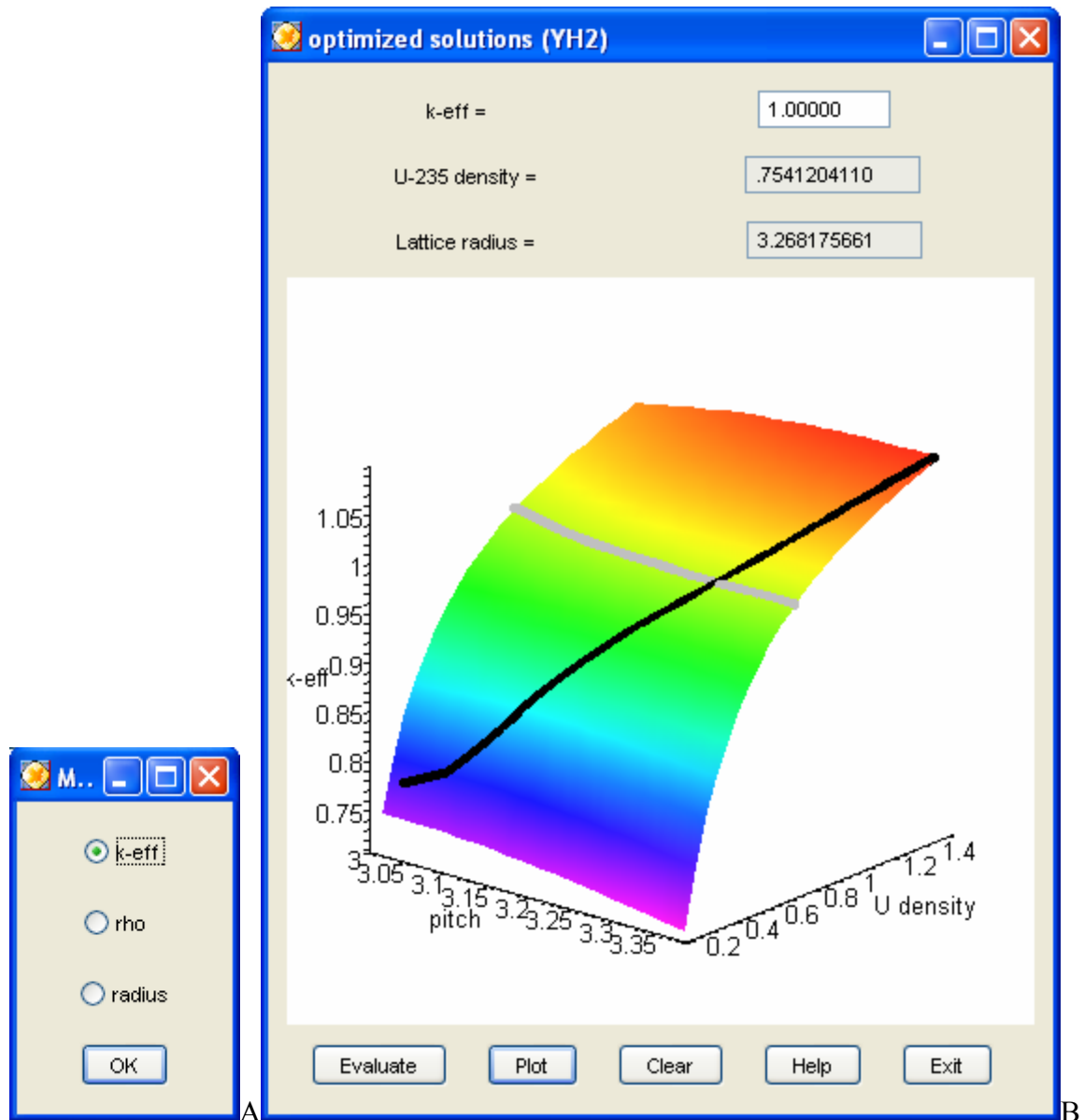


Figure 5-1. Data delivery maplet for the YH₂ moderated reactor. A) Initial Prompt. B) user interface.

Object 5-1. ZrH₂ reactor data delivery maplet

Object 5-2. YH₂ reactor data delivery maplet

Future Work

Additional work should be done to further evaluate this design. It would be advantageous to obtain data for systems with other fuel porosities in addition to 50%. Of special importance is the need to perform detailed heat transfer studies to evaluate the possibility of an uncontrolled reactivity excursion due to the positive moderator temperature defect. The gap between the fuel and the moderator should aid in preventing a large increase in the moderator temperature from a transient in the fuel, but this is difficult to say at this point. A detailed study in this area should address whether the fuel's negative reactivity coefficient and the importance of delayed neutrons is enough to offset the moderator's positive reactivity coefficient in preventing an excursion. If a reactivity excursion is indeed likely, it would be necessary to determine if it occurs slowly enough so a computer can correct for it through control drum rotation.

APPENDIX A INPUT FILE FOR MCNP

```

Foam fuel -- 5cm OD & 2cm ID 0.365gu/cc 50% porosity optimized at 3.493
cm pitch
1 0 -1                               imp:n=1 U=5 $ inner coolant
2 2 -3.538815047 1 -2                 imp:n=1 U=5 $ fuel foam
3 0 2 -3                               imp:n=1 U=5 $ outer coolant
4 3 -5.47 3                           imp:n=1 U=5 $ YH2 moderator
5 3 -5.47 -4 5 -6 -7 -8 -9           imp:n=1 U=2 lat=2 $just mod
6 0 -4 5 -6 -7 -8 -9                 imp:n=1 U=1 lat=2 fill=5 $just mod
7 0 -4 5 -6 -7 -8 -9                 imp:n=1 U=3 lat=2 fill=-5:5 -5:5 0:0
    2 2 2 2 2 2 2 2 2 2 2 2
      2 2 2 2 2 2 2 2 2 2 2 2
        2 2 2 2 2 2 2 2 2 2 2 2
          2 2 2 2 2 1 1 1 2 2 2
            2 2 2 2 1 1 1 1 2 2 2
              2 2 2 1 1 1 1 1 2 2 2
                2 2 2 1 1 1 1 2 2 2 2
                  2 2 2 1 1 1 2 2 2 2 2
                    2 2 2 2 2 2 2 2 2 2 2
                      2 2 2 2 2 2 2 2 2 2 2
                        2 2 2 2 2 2 2 2 2 2 2
7 0 -10 13 -12                       imp:n=1 fill=3
9 4 -3.01 (10:12:-13) -14 -11 15 20 21 22 23 24 25 imp:n=1 $ BeO
reflector
c -----control drums-----
10 4 -3.01 -20 -30 -14 15  imp:n=1
11 4 -3.01 -21 -31 -14 15  imp:n=1
12 4 -3.01 -22 -32 -14 15  imp:n=1
13 4 -3.01 -23 -33 -14 15  imp:n=1
14 4 -3.01 -24 -34 -14 15  imp:n=1
15 4 -3.01 -25 -35 -14 15  imp:n=1
c
20 5 -2.52 -20 30 -14 15  imp:n=1
21 5 -2.52 -21 31 -14 15  imp:n=1
22 5 -2.52 -22 32 -14 15  imp:n=1
23 5 -2.52 -23 33 -14 15  imp:n=1
24 5 -2.52 -24 34 -14 15  imp:n=1
25 5 -2.52 -25 35 -14 15  imp:n=1
c
55 0 (11:14:-15) (20:14:-15)
    (21:14:-15) (22:14:-15)
    (24:14:-15) (25:14:-15)
        (23:14:-15)                imp:n=0 $ void

1 cz 0.5      $ inner fuel radius
2 cz 2.5      $ outer fuel radius
3 cz 2.549    $ outer flow radius
c -----lattice planes-----

```

```

4 py 3.4927
5 py -3.4927
6 p 2.016511285 3.4927 0 2.016511285 3.4927 1 4.03302257 0 0
7 p -2.016511285 -3.4927 0 -2.016511285 -3.4927 1 -4.03302257 0 0
8 p 2.016511285 -3.4927 0 2.016511285 -3.4927 1 4.03302257 0 0
9 p -2.016511285 3.4927 0 -2.016511285 3.4927 1 -4.03302257 0 0
c -----Core top, bottom, reflector-----
10 cz 17.8635
11 cz 37.8635
12 pz 17.8635
13 pz -17.8635
14 pz 37.8635
15 pz -37.8635
c -----Control drums-----
20 c/z 0 27.9024303 10.02893
21 c/z 24.16421347 13.95121515 10.02893
22 c/z 24.16421347 -13.95121515 10.02893
23 c/z 0 -27.9024303 10.02893
24 c/z -24.16421347 -13.95121515 10.02893
25 c/z -24.16421347 13.95121515 10.02893
c -----planes in the drums-----
30 p 0 37.84403485 0 0 37.84403485 1 1 37.84403485 1
31 p 32.77389556 18.92201742 0 32.77389556 18.92201742 1
    33.27389556 18.05599202 1
32 p 32.77389556 -18.92201742 0 32.77389556 -18.92201742 1
    32.27389556 -19.78804283 1
33 p 0 -37.84403485 0 0 -37.84403485 1 -1 -37.84403485 1
34 p -32.77389556 -18.92201742 0 -32.77389556 -18.92201742 1
    -33.27389556 -18.05599202 1
35 p -32.77389556 18.92201742 0 -32.77389556 18.92201742 1
    -32.27389556 19.78804283 1

mode n
kcode 4000 1.0 20 1000 4000      $ 20 inactive 100 active
ksrc 0.0 1.5 0.0
TMP:n      0 2.5851e-7 0 6.8936e-8 6.8936e-8 0 0 0
           5.1702e-8 5.1702e-8 5.1702e-8 5.1702e-8
           5.1702e-8 5.1702e-8 5.1702e-8
           5.1702e-8 5.1702e-8 5.1702e-8
           5.1702e-8 5.1702e-8 5.1702e-8
FMESH4:n  GEOM=cyl IMESH=17.8635 IINTS=100 JMESH=-17.8635 17.8635
           KMESH=1 KINTS=100 EMESH 0.625e-6, 1e-3
           EINTS= 1 1 OUT=ik

c
m2      92235.65c 0.0008888
        92238.65c 0.0000275
        40000.60c 0.0292010
        41093.60c 0.0097337
        6000.60c 0.0398509

mt2     grph.08t          $2000 K graph, fuel @ 3000
c
m3      40000.60c 1          $ ZrH2 moderator
        1001.60c 2
mt3     h/zr.63t          $ H in ZrH2 @ 800 K
        zr/h.63t          $ Zr in ZrH2 @ 800 K
c
m4      4009.60c .5          $ BeO

```

	8016.60c	.5	\$ BeO
mt4	beo.62t		\$ BeO at 600 K
c			
m5	5010.60c	4	\$ B4C absorber
	6000.60c	1	

APPENDIX B INTERPOLATING ALGORITHM IN MAPLE

```

M:=Matrix(<<.1|.45485>,<.2|.65272>,<.3|.76376>,<.35|.80407>,<.4|.8362>,<.5|.887
15>,<.75|.96761>,<1|1.01391>,<1.25|1.04588>,<1.5|1.07149>>):

H:=Matrix(<<3|1.05785>,<3.1|1.07473>,<3.2|1.08516>,<3.3|1.09026>,<3.4|1.09057>,<3.5|1.0861>,<3.6|1.07799>,<3.7|1.06679>,<3.8|1.05413>,<3.9|1.03723>,<4|1.02005
>>):

L:=Matrix(<<3|.85873>,<3.1|.86289>,<3.2|.86135>,<3.3|.85523>,<3.4|.84577>,<3.5|.83212>,<3.6|.81805>,<3.7|.80035>,<3.8|.78349>,<3.9|.76348>,<4|.74318>>):
  high:=spline([seq(H[i,1],i=1..11)],[seq(H[i,2],i=1..11)],x,3):
  low:=spline([seq(L[i,1],i=1..11)],[seq(L[i,2],i=1..11)],x,3):

f:=spline([seq(M[i,1],i=1..10)],[seq(M[i,2],i=1..10)],x,3):

new:=(high*(subs(x=y,f)-eval(f,x=.35))+low*(eval(f,x=1.5)-
subs(x=y,f)))/(eval(f,x=1.5)-eval(f,x=.35)):

for i from 1 by 1 to 15 do
part[i]:=plot(eval(new,y=i/10),x=3..4);
end do:

> opt:=Vector(1000):
> Y:=Vector(1000):
> j:=0:

for y from 0.23 by 0.01 to 1.5 do
j:=j+1:
Y[j]:=y:
opt[j]:=fsolve(diff(new,x)=0,x=3..4);
end do:
unassign('y'):
> optimized:=spline([seq(Y[i],i=1..128)],[seq(opt[i],i=1..128)],x,3):
>
optk:=spline([seq(Y[i],i=1..128)],[seq(eval(subs(y=Y[i],x=opt[i],new)),i=1..128
)],x,3):
>
> getr:=proc(a)
eval(subs(x=a,optimized));
end proc:
> getk:=proc(a)
eval(subs(x=a,optk));
end proc:
> getrhofromk:=proc(a)
fsolve(optk=a,x=0.1..1.5);
end proc:

```

LIST OF REFERENCES

1. Anghaie S, Knight T-W: *Status of Advance Carbide Fuels: Past, Present, and Future* (p. 852-856). Proceedings of the Space Technology and Applications International Forum (STAIF), ed. M. S. El-Genk, AIP Conf. Proceedings, 608, AIP, New York, 2002.
2. Youchison D-L, Lenard R-X, Williams B-E, Anghaie S: 2005: *Development of a Tricarbide Foam Fuel Matrix for Nuclear Propulsion*. Proceedings of the space nuclear conference, 2005.
3. Lenard R-X, Youchison D-L: *Analysis of a Reticulated Vitreous Foam Nuclear Thermal Rocket Reactor Core*. Proceedings of the space nuclear conference, 2005.
4. X-5 Monte Carlo Team: *MCNP – A General Monte Carlo N-Particle Transport Code, Version 5*. Los Alamos National Lab, Los Alamos, NM, 2003.
5. *MONTEBURNS 2.0 An Automated, Multi-Step Monte Carlo Burnup Code System*. Los Alamos National Laboratory, Los Alamos, NM, 2003.

BIOGRAPHICAL SKETCH

Eddy Perez Cardentey was born in Cuba on January 2nd, 1980. After migrating to the United States on February 2nd, 1995 he enrolled in the International Baccalaureate (IB) program at Suncoast Community High School in Riviera Beach, Florida. He graduated 2 years later with an International Baccalaureate diploma, and an Advanced Placement diploma. He attended the University of Florida since 1997, where he obtained a Bachelor of Science in Nuclear Engineering in December 2002 and a Master of Science in August 2005.